Multiple-Differential Encoding for Multi-Hop Amplify-and-Forward Relaying in IR-UWB Systems

by

Maziyar Hamdi

B.Sc., Sharif University of Technology, Tehran, Iran, 2007

A THESIS SUBMITTED IN PARTIAL FULFILLMENT OF
THE REQUIREMENTS FOR THE DEGREE OF

MASTER OF APPLIED SCIENCE

in

The Faculty of Graduate Studies

(Electrical and Computer Engineering)

THE UNIVERSITY OF BRITISH COLUMBIA

(Vancouver)

February 2010

Abstract

In this thesis, we propose to improve the performance and coverage of impulse-radio ultra-wideband (IR-UWB) systems by means of cooperative multi-hop relaying. With regard to a simple practical realization, we focus on a non-coherent system setup in conjunction with amplify-and-forward (A&F) relaying. In particular, we propose to employ a multiple-differential encoding scheme at the source node and single differential decoding at each relay and at the destination node, respectively, so as to efficiently limit intersymbol-interference (ISI) effects at the destination node. A thorough performance analysis of the proposed scheme is provided, along with a closed-form optimization of the transmit power allocation to the source node and the relays. Simulation results illustrate the excellent performance of the proposed scheme, which is also compared to alternative coherent and non-coherent multi-hop IR-UWB schemes based on A&F relaying and decode-and-forward (D&F) relaying.

Table of Contents

Appendices

List of Tables

List of Figures

List of Abbreviations

AWGN	Additive white Gaussian noise
A&F	Amplify-and-forward
BER	Bit error rate
CDMA	Code division multiple access
CIR	Channel impulse response
D&F	Decode-and-forward
DF	Differential
DS-SS	Direct sequence spread spectrum
EGC	Equal gain combining
FCC	Federal Communications Commission
FEC	Forward error correction
GPS	Global positioning system
IPI	Interpulse interference
IR	Impulse radio
ISI	Intersymbol-interference
MAI	Multiple access interference
MB-OFDM	Multiband orthogonal frequency-division multiplexing
MC	Multi-carrier
MRC	Maximum ratio combining

PSD	Power spectral density
RF	Radio frequency
S-D	Source-Destination
SNR	Signal-to-noise ratio
TH	Time-hopping
TR	Transmitted reference
UWB	Ultra wideband
WPAN	Wireless personal area network

Acknowledgments

I owe my deepest gratitude to my supervisor, Dr. Robert Schober, for the constant guidance and support that he has provided. This thesis would not have been possible without his helpful suggestions, advice and constant encouragement.

I would also like to thank Dr. Jan Mietzner for his support of and helpful comments on my research. I would like to extend my thanks as well to all of my friends and colleagues in the communication group for creating a friendly and productive environment.

Furthermore, a heartfelt and deep thanks go to my family, and especially my brother Mazda, who have always encouraged me and given their unconditional support throughout my studies at the University of British Columbia. Without their support I could not have completed this thesis.

Maziyar Hamdi

The University of British Columbia

February 2010

Dedication

To my parents...

Chapter 1

Introduction

In this chapter, first a brief overview of ultra-wideband (UWB) technology is provided in Section 1.1. After that, in Section 1.2, different types of UWB receivers are discussed and some approaches in the literature for performance improvement of these receivers are summarized. Section 1.3 gives a literature survey about cooperative diversity with emphasis on its applications in UWB systems. Then, in Sections 1.4 and 1.5, respectively, we summarize the contributions and outline the organization of thesis. Finally, publications related to this thesis are listed in Section 1.6.

1.1 Ultra-wideband Communication

UWB is a wireless spectral underlay technology for transmitting signals with a bandwidth larger than 500 MHz or a fractional bandwidth of more than 20%. Here, the fractional bandwidth is defined by B/f_c, where B and f_c denote the -10 dB bandwidth and the centre frequency [1–4], respectively. Furthermore, $B = f_H - f_L$, and $f_c = \frac{f_H+f_L}{2}$, where f_H and f_L are the higher and lower frequencies for -10 dB gain [3], respectively. The above definition of UWB signals implies that in UWB communication systems with a centre frequency, f_c, greater than 2.5 GHz the signal bandwidth should be larger

than 500 MHz. For lower centre frequencies, the bandwidth has to satisfy $B/f_c > 0.02$ [5].

Owing to their large bandwidth, UWB transmission techniques are, for example, envisioned for short-range high-speed indoor communications. Due to the favorable characteristics of UWB communications such as low-cost, simple implementation, and high data rates, UWB-based systems are being used in many applications such as wireless personal area networks (WPAN), sensor networks, and vehicular radar systems. Currently, there are three different standards or standard proposals for UWB radio [6], which are quite different in nature, namely (i) the ECMA-368 standard [7], which is based on a multiband orthogonal frequency-division multiplexing (MB-OFDM) modulation scheme, (ii) the direct-sequence (DS) UWB standard proposal [8], which is based on a DS spread-spectrum (DS-SS) scheme, and (iii) the IEEE 802.15.4a standard [9], which is based on the (rather traditional) impulse-radio (IR) technique. In multicarrier (MC) based UWB systems, the concepts in direct-sequence spread spectrum (DS-SS) or code-division multiple-access (CDMA) are expanded with MC techniques. Conventional DS-SS can also be used to produce a UWB signal if a sufficiently high chip rate issued. MC schemes have a higher receiver complexity because of multi-stage mixing or Fourier transform [6].

Impulse radio is another form to implement time-modulated UWB. In IR-based UWB (IR-UWB) systems, the transmitted signal consists of a train of pulses of very short duration [10]. By this means, an ultrawide bandwidth is generated, without requiring any additional carrier modulation. One of the most attractive characteristics of IR-UWB systems is their

low complexity because of their baseband nature . An UWB transmitter can send data by modulating short pulses and radio frequency (RF) mixing is not required [11]. So the implementation of IR-UWB systems is low-cost compared with conventional communications systems. As a result of these ultra short pulses, IR-UWB is widely used for high speed and high data rate communications. Hundreds of mega bit per second (Mbps) are achievable with IR-UWB communication systems. Due to its simple practical realization and its robustness to multipath fading and intersymbol-interference (ISI) effects, IR-UWB has attracted considerable attention. Moreover, by deploying pseudo-random time-hopping (TH) sequences, IR-UWB can also support multiuser communications with a minimum of multiple-access interference (MAI).

1.2 UWB Receivers

The US Federal Communications Commission (FCC) has introduced tight limitations (below -41.3 dBm/Hz) on the transmitted power spectral density (PSD) of UWB systems to restrict interference to incumbent wireless services [5]. The FCC spectral mask, Fig. 1.1, allows UWB systems to operate in frequency bands that have been allocated to licensed narrowband systems. For example, in the 960 MHz-1.61 GHz band, where the global positioning system (GPS) operates, UWB system can send data with a power level lower than -76.3 dBm.

Because of these limitations, it is essential to capture at the receiver most of the signal energy provided by the large number of resolvable multipath

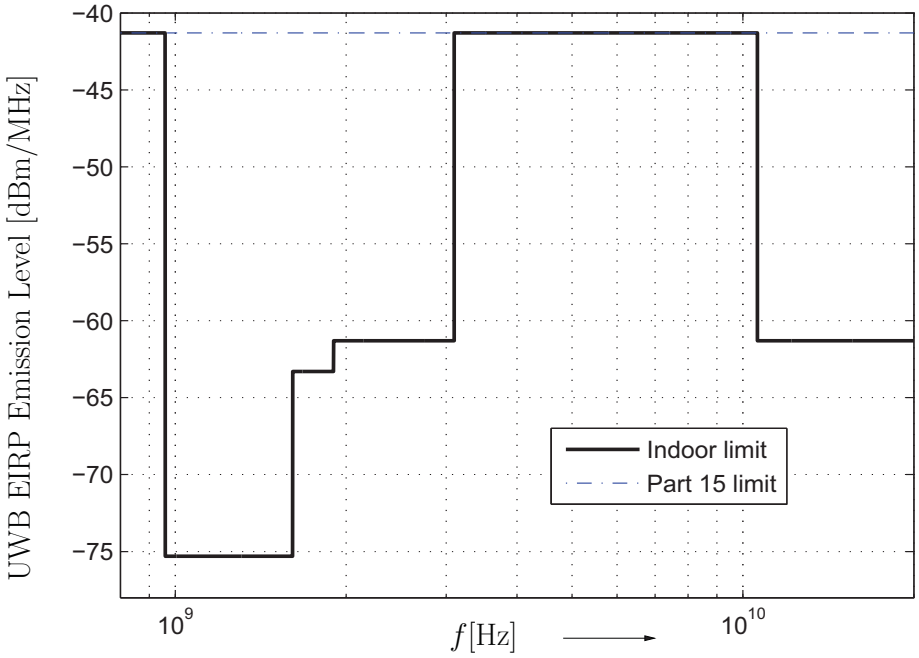

Figure 1.1: FCC spectral mask for indoor communication systems

components. A favorable property of IR-UWB systems is that they allow for an efficient energy combining at the receiver [12] – either by means of coherent Rake combining [13] or non-coherent energy detection schemes [14, 15]. In the case of Rake combining, the received signal is correlated with an appropriate template signal, which is designed for coherent combination of the energies of the individual multipath signal components. An ideal all-Rake (A-Rake) receiver captures the energy of all resolvable multipath components and thus offers optimum performance in terms of bit error rate (BER). However, it requires accurate channel estimation at the receiver and

precise timing synchronization, which might be challenging in practice. In particular, a large number of "Rake fingers" is typically required in order to capture the entire signal energy [16]. As opposed to this, partial Rake (P-Rake) and selective Rake (S-Rake) combiners collect only part of the signal energy, thus providing suboptimal performance at the benefit of a reduced receiver complexity. Still, accurate channel knowledge and precise timing synchronization are indispensable. In S-Rake receivers, the L_s most significant multi-path components are collected while the P-Rake receiver combines the L_p first multi-path components.

As opposed to this, non-coherent energy detection schemes relieve the receiver from any channel estimation task and are thus easier to realize in practice. They capture the energy of the multipath components by means of an autocorrelation of the received signal, followed by an integrate-and-dump operation. Among these techniques, differential (DF) and transmitted-reference (TR) schemes are the most popular options [14]. In the TR scheme, pulses are transmitted in pairs, where the first pulse serves as reference pulse and the second pulse, which follows the reference pulse with a fixed delay, is modulated by the transmitted information bit sequence. At the receiver, the reference pulse serves as a noisy template for the autocorrelation process, so that the transmitted information bit modulated onto the second pulse can be recovered by means of the subsequent integrate-and-dump operation. In the DF scheme, however, the information bit sequence is differentially encoded at the transmitter, and the autocorrelation process at the receiver (in conjunction with the integrate-and-dump operation) performs the corresponding differential decoding step. A notable advantage of the DF scheme

is that it offers a higher data rate compared to a TR scheme [14], since the additional template pulse can be discarded. In the literature, several methods have been proposed to improve the performance of DF schemes, such as reference filtering [17], weighted correlation [18], and multiple symbol detection [19].

1.3 Cooperative Diversity in UWB Systems

Cooperative diversity is another way to overcome the limited coverage of (coherent or non-coherent) UWB systems [20, 21]. The idea of cooperative diversity was first proposed in [22] and [23]. Through cooperative diversity, wireless network terminals can create redundancy by relaying message for each other. The receiver at the destination can use these redundant signals to overcome multi-path fading and shadowing. Cooperative diversity improves network performance and improves the achievable rate by use of different cooperative diversity protocols. Two popular schemes for cooperative relaying are amplify-and-forward (A&F) and decode-and-forward (D&F) relaying. A&F relays simply amplify and re-transmit the received signal, whereas D&F relays first decode and then re-encode the received signal, before re-transmission is performed [24]. Correspondingly, D&F relaying is more complex than A&F relaying, especially if a forward-error-correction (FEC) code is employed. The diversity gain of A&F and D&F relay was investigated in [25]. Coherent and non-coherent receivers for these schemes were described in [26] and [27], respectively. End-to-end performance, BER, and outage probability in Rayleigh fading channels for a simple two-hop sys-

tem were investigated in [28]. The performance analysis has been extended to Nakagami fading in [29].

1.4 Thesis Contributions

In this thesis, we investigate the use of relays to overcome the limited coverage of (coherent or non-coherent) UWB systems [20, 21, 30–32]. Instead of transmitting signals directly from a source node, S, to a destination node, D, the signal is (in the simplest case) received by an intermediate relay, R_1, which forwards the received signal from the source node to the destination node. In a more complicated multi-hop scenario consisting of m subsequent links, the source signal is forwarded between $(m-1)$ relays R_1, ..., R_{m-1}, before it finally reaches the destination node. With relaying, substantial path-loss gains can be provided due to shorter link lengths. Available relays can either be dedicated relays, which do not disseminate any data of their own, or temporarily inactive IR-UWB devices acting as relays, so as to assist the current source-destination link.

Previous work on relaying for UWB systems has focused on the ECMA-368 UWB standard [20, 21], space time-code design for coherent IR-UWB systems [30], coherent A&F and D&F relaying requiring a Rake combiner at each relay [31, 32], and dual-hop D&F relaying for IR-UWB with single-differential encoding at the source [32].

For the sake of a simple practical realization, we will focus on a combination of the DF IR-UWB scheme with A&F relaying. A straightforward combination of the two techniques with differential encoding at the source

node, simple A&F relaying at the intermediate relay(s), and differential decoding at the destination node has the major drawback that the length of the effective overall channel impulse response (CIR) increases with each hop. Compared to direct transmission (i.e., without any relaying), significantly larger guard intervals between the transmitted pulses are therefore required, in order to achieve a similar level of ISI. Otherwise, the increased amount of ISI will severely limit the overall performance and can even compromise the achieved path-loss gains. Note that an increased guard interval will significantly lower the effective data rate compared to direct transmission. As an alternative, we propose a *multiple-differential* encoding setup with m-fold differential encoding at the source node in conjunction with single differential decoding at each A&F relay and at the destination node. By this means, the same level of ISI is achieved as in the case of direct transmission, without requiring an extended guard interval. To the best of our knowledge, such a use of multiple-differential encoding is novel and quite different from narrowband systems, where, for example, double-differential encoding is employed to mitigate carrier frequency offsets [33].

The main contributions of this thesis are as follows:

- We propose the use of double differential encoding at the transmitter for dual-hop relaying to limit ISI without any loss in terms of data rate.
- For the dual-hop case we derive a simple closed-form expression for the power allocation factors for the transmitter and the relay, which only depends on the length of source-relay and relay-destination links.

- We generalize the idea of using differential encoding in order to mitigate ISI to multi-hop UWB systems and propose to use multiple differential encoding at the transmitter.
- We derive a recursive formula for the signal-to-noise ratio (SNR) at the destination for the multi-hop case.
- We propose a sub-optimal, recursive approach for optimizing the power allocation factors in multi-hop UWB systems.

1.5 Thesis Organization

The rest of the thesis is organized as follows. In Chapter 2, we describe the system setup. The structures of transmitter, channel, relay, and receiver for multi-hop transmission are discussed in this chapter. In Chapter 3, we consider a dual-hop system and analyze its performance in terms of SNR and derive a closed-form expression for the optimum power allocation which maximizes the SNR at the destination. A recursive formula for the SNR of multi-hop IR-UWB systems and a sub-optimal approach for optimizing the corresponding power allocation factors at the source and the relays are provided in Chapter 4. In Chapter 5, the structure of the Rake receiver is reviewed and the optimum power allocation for dual-hop transmission with Rake combining is derived. Simulation results, which illustrate the excellent performance of our scheme, are presented in Chapter 6. Finally, Chapter 7 concludes the thesis and presents possible directions for future work.

1.6 Related Publications

- M. Hamdi, J. Mietzner, and R. Schober: Double Differential Encoding for Dual-Hop Amplify-and-Forward Relaying in IR-UWB Systems. *Accepted for presentation at IEEE Vehicular Technology Conference (VTC). Taipei, Taiwan, March 2010*

- M. Hamdi, J. Mietzner, and R. Schober: Multiple Differential Encoding for Multi-Hop Amplify-and-Forward Relaying in IR-UWB Systems. *To be submitted to IEEE Transactions on Wireless Communications. Manuscript is* 95 *% complete.*

Chapter 2

System Model

Throughout this thesis, we consider a serial multi-hop DF IR-UWB system consisting of a source node S, $(m-1)$ A&F relays $R_1, ..., R_{m-1}$, and a destination node D. Here, $m>1$ denotes the total number of hops. The link between source S and relay R_1 is in the sequel denoted as Link 1, the link between relay R_{i-1} and relay R_i is denoted as Link i $(2 \leq i \leq m-1)$, and the link between the last relay R_{m-1} and the destination node D is denoted as Link m. For the ease of exposition, we focus on the single-user case here.

Before we provide a detailed description of the system setup, including the underlying channel model as well as the structures of the source node, the relay node(s), and the destination node, we briefly recapitulate the IR-UWB transmission format and highlight the advantages of our proposed multiple-differential A&F relaying scheme.

2.1 IR-UWB Transmission Format

In IR-UWB systems, the transmitted signal consists of a train of ultra-short pulses (on the order of nanoseconds), which are modulated by the transmitted information symbols [10]. Within the scope of this thesis, focus will be on pulse-amplitude modulation (PAM). As illustrated in Fig. 2.1 (a), $N_f \geq 1$

frames are used to convey a single information symbol (in the example, we have $N_f = 2$). By this means, the effective symbol energy at the receiver can be increased, however, at the expense of a decreased throughput. After transmission, the IR-UWB signal is convolved with the UWB CIR, which can have a length on the order of hundreds of nanoseconds [4], depending on the radio environment under consideration. Correspondingly, the received pulses are considerably spread out in time, cf. Fig. 2.1 (b). In the DF setup, the energy of the underlying multipath signal components is collected at the receiver by means of the integrate-and-dump operation (for details see Section 2.4).

If a straightforward combination of the IR-UWB transmission format with A&F relaying is employed, the effective CIR seen at the destination node results from a convolution of the UWB CIRs of all intermediate links. Correspondingly, the time spread of the received pulses will grow with each hop, leading to significant interpulse interference (IPI) and ISI, as the received pulses associated with one information symbol (i.e., with one set of N_f frames) interfere with those associated with the subsequent symbol. In order to keep the level of IPI and ISI comparable to the single-hop case, the only option is to increase the guard intervals between subsequent pulses and symbols, which will (further) decrease the effective throughput.

In the following, we present the details of our proposed multiple-differential A&F relaying scheme. A major advantage of our scheme is that the level of IPI and ISI is not increased compared to the single-hop case. In particular, since differential decoding (in conjunction with the integrate-and-dump operation) is performed at each relay, the time spread of the received pulses

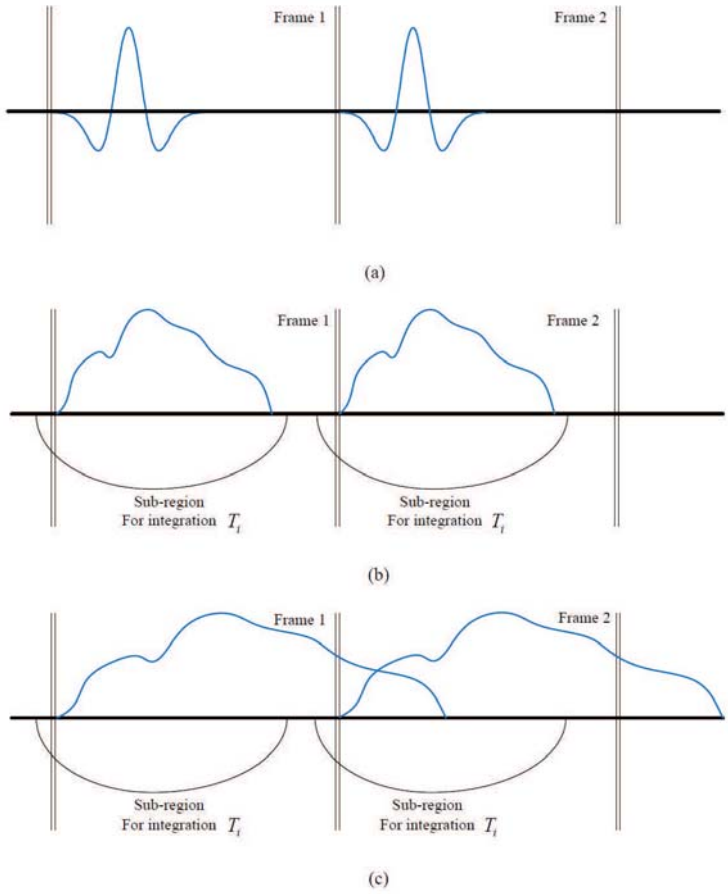

Figure 2.1: Effects of relaying in straightforward dual-hop A&F IR-UWB: (a) transmitted signal, (b) received signal after one hop, and (c) received signal after two consecutive hops without intermediate differential decoding.

depends only on a single UWB CIR, so that the same guard interval size can be employed as in the case of a single hop.

2.2 Proposed Structure of Source Node

Fig. 2.2 shows the proposed structures of the source node S, the ith A&F relay R_i, and the destination node D. Throughout this thesis, the employed relays $R_1, ..., R_{m-1}$ are assumed to have identical structures. We start with a description of the source node structure.

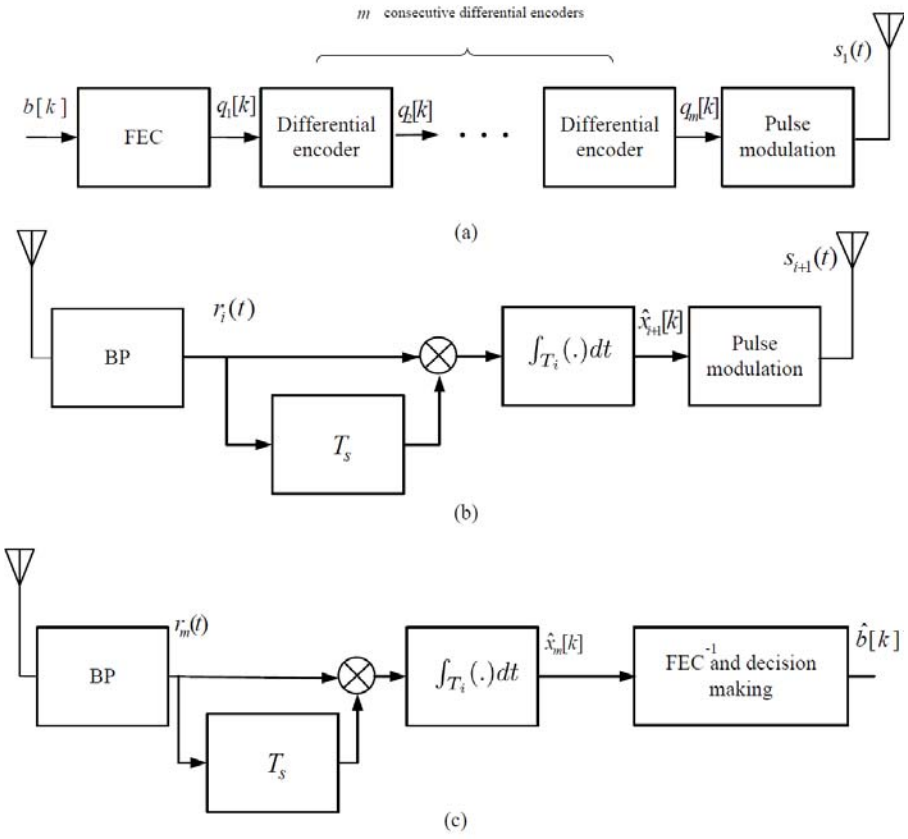

Figure 2.2: Block diagram of the (a) transmitter, (b) relay, and (c) destination.

At the source node, the transmitted information bits, $b[\kappa] \in \{0, 1\}$, are

(possibly) first encoded by a forward-error-correction (FEC) encoder (see Fig. 2.2 (a)), which yields coded bits $c[k]$. These are then mapped onto binary antipodal symbols $q_1[k] \in \{\pm 1\}$, according to the mapping rule $0 \mapsto -1,\ 1 \mapsto +1$. Next, the information symbols $q_1[k]$ are m-times differentially encoded according to

$$q_r[k] = q_{r-1}[k] q_r[k-1], \qquad 2 \leq r \leq m+1, \tag{2.1}$$

where $q_r[k] \in \{\pm 1\}$ denotes the kth intermediate symbol after the $(r-1)$th differential encoder ($2 \leq r \leq m+1$). The symbols $q_{m+1}[k]$ are then modulated onto a train of (real-valued) short pulses $w_{tx}(t)$ with duration T_p, according to [3]

$$s_1(t) = \sqrt{\alpha_1 E_g} \sum_{k=-\infty}^{\infty} \sum_{j=0}^{N_f-1} q_{m+1}[k]\, w_{tx}(t - jT_f - kT_s). \tag{2.2}$$

Here, $s_1(t)$ denotes the transmitted signal, α_1 the transmit power allocation factor for the source node, E_g the energy per pulse ($\int_{-\infty}^{+\infty} w_{tx}^2(t)\, dt := 1$), N_f the number of frames used for conveying a single information symbol, T_f the frame duration, which is chosen much larger than the pulse duration (i.e., $T_f \gg T_p$), and $T_s := N_f T_f$ the symbol duration. The effective bit rate is given by $R_b := 1/T_s$. The length of the guard interval between subsequent pulses and subsequent symbols, $T_g := T_f - T_p$, is typically chosen longer than the (expected) length of the UWB CIR, so as to circumvent IPI and ISI effects.

2.3 Channel Model

In the following, Link i denotes the link between node (i) and node $(i+1)$. For all links under consideration, we employ the IEEE 802.15.3a channel models [34] for UWB personal area networks. Consequently, the passband version of the CIR of the rth link consists of L_C clusters of L_R rays and is modeled as

$$h_r(t) = \sum_{\nu=0}^{L_C} \sum_{\mu=0}^{L_R} \lambda_{\mu,\nu}^{(r)} \, \delta(t - T_\nu^{(r)} - \tau_{\mu,\nu}^{(r)}), \tag{2.3}$$

where $\lambda_{\mu,\nu}^{(r)}$ models the random multipath gain coefficient of the μth ray of the νth cluster, $T_\nu^{(r)}$ the delay of the νth cluster, $\tau_{\mu,\nu}^{(r)}$ the delay of the μth ray of the νth cluster, and $\delta(\cdot)$ denotes a Dirac impulse. The multipath gain coefficients are normalized such that $\sum_{\nu=0}^{L_C} \sum_{\mu=0}^{L_R} \lambda_{\mu,\nu}^{2(r)} = 1$. In [34], four different parameter sets are specified for the various parameters in (2.3). The resulting channel models, CM1-CM4, represent different usage scenarios and entail different amounts of IPI and ISI.

Fig. 2.3 shows one hundred realizations of the CIR of an UWB link for model CM1. Fig. 2.4 depicts the average power decay profile versus delay time. As shown in these figures, the maximum excess delay is about 60 ns so with a guard interval of about 70 ns, effects of ISI can be mitigated.

The channel gain is affected by log-normal fading and path loss, which is usually modeled in the UWB literature according to [35, 36]

$$G(d) = G_0 + 10 \cdot p \log(d_0/d) + \chi, \tag{2.4}$$

where $G(d)$ denotes the channel gain in dB, d the link length in meter, G_0

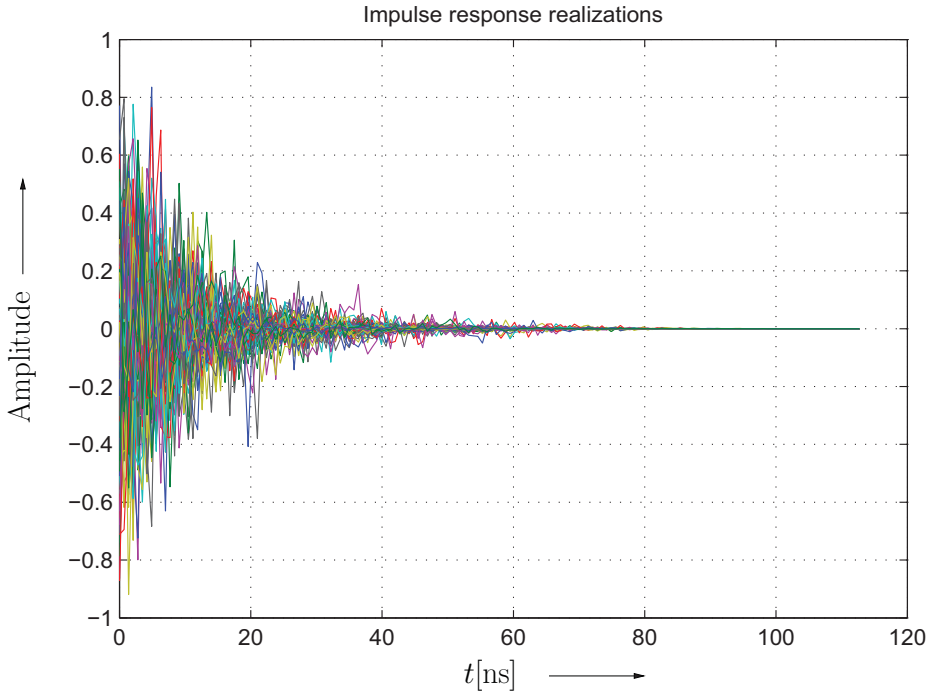

Figure 2.3: Different channel realizations for CM1 model.

the channel gain resulting for some reference distance d_0 (e.g., $d_0 = 1\text{m}$), p the path-loss exponent, and χ a log-normal fading term. In the following, the source-destination (S-D) link will serve as a reference link for the path loss, in order to allow for a fair comparison between the proposed multi-hop relaying setup and the case of direct transmission. Assuming omni-directional antennas at all nodes, the relative channel gain associated with the ith link is thus modeled by a factor [21]

$$A_i := \chi_i \left(\frac{d_{S-D}}{d_i} \right)^p , \tag{2.5}$$

Figure 2.4: Power decay profile versus delay for CM1 channel model.

where χ_i models the log-normal fading associated with the ith link, and d_{S-D} and d_i denote the lengths of the source-destination link and the ith link, respectively. The path-loss exponent p is typically between $1.7 \leq p \leq 3.5$ [34]. Throughout this thesis, we assume that the lognormal shadowing terms χ_i and $\chi_{i'}$ associated with two different links $i \neq i'$ are uncorrelated.

2.4 Proposed A&F Relay Structure

At the receiver front-end of each relay, the received signal is first passed through a bandpass filter $h_{BP}(t)$ with one-sided bandwidth W, so as to

eliminate out-of-band noise (see Fig. 2.2 (b)). The filtered received signal at the first relay is given by

$$\begin{aligned} r_i(t) &= \sqrt{A_i}\left(h_i(t) * h_{BP}(t)\right) * s_i(t) + n_i(t) \\ &= \sqrt{A_i \alpha_i E_g} \sum_{k=-\infty}^{\infty} \sum_{j=0}^{N_f-1} \xi_i[k]\, w_{rx,i}(t - jT_f - kT_s) + n_i(t), \quad (2.6) \end{aligned}$$

where A_i is the relative channel gain associated with Link i, $h_i(t)$ the corresponding CIR, $s_i(t)$ the transmitted signal of the source node ($i=1$) or the $(i-1)$th relay ($1<i<m-1$), $n_i(t)$ the filtered additive white Gaussian noise (AWGN) with zero mean and single-sided noise PSD $\frac{N_0}{2}$, α_i the transmit power allocation factor for the source node ($i=1$) or the $(i-1)$th relay ($1<i\leq m-1$), $w_{rx,i}(t)=w_{tx}(t)*h_i(t)*h_{BP}(t)$ the received pulse associated with Link i, and '$*$' denotes linear convolution. Moreover,

$$\xi_i[k] := \begin{cases} q_{m+1}[k] & \text{for} \quad i=1 \\ \hat{x}_{i-1}[k] & \text{for} \quad 1<i<m-1 \end{cases}, \quad (2.7)$$

where $q_{m+1}[k]$ denotes the kth transmitted symbol of the source node and $\hat{x}_{i-1}[k]$ the soft estimate of the kth intermediate symbol $q_{m-i+2}[k]$ formed at the $(i-1)$th relay ($1<i<m-1$), see details below. For the numerical results presented in Chapter 6, the bandwidth W of the bandpass $h_{BP}(t)$ was optimized numerically for maximization of the SNR.

After the bandpass filter, (single) differential decoding of the filtered receive signal $r_i(t)$ is performed. To this end, signal $r_i(t)$ is first delayed by a symbol duration T_s and is then multiplied by itself. The resulting

signal $r_i(t)r_i(t-T_s)$ is passed through an integrator with basic integration duration T_i.[1] Throughout this thesis, we assume perfect synchronization of the relays and the destination node with respect to the employed frame structure [14]. In particular, the overall integration time is composed of N_f separated sub-region intervals (one per received frame), as shown in Fig. 2.1. By this means, the negative impact of the additive noise can be efficiently limited (e.g., in comparison to a single integration interval of length $N_f T_f$). The integrator yields the discrete-time output sample

$$\hat{x}_i[k] = \sum_{j=0}^{N_f-1} \int_{kT_s+jT_f}^{kT_s+jT_f+T_i} r_i(t) r_i(t-T_s) dt, \tag{2.8}$$

which can be interpreted as a (soft) estimate of the intermediate symbol

$$q_{m-i+1}[k] = q_{m-i+2}[k] \cdot q_{m-i+2}[k-1] \tag{2.9}$$

(due to the differential decoding step, see Chapter 3 for further details). Similar to (2.2), the estimated symbols $\hat{x}_i[k]$ are finally modulated onto a signal

$$s_{i+1}(t) = \sqrt{\alpha_{i+1} E_g} \sum_{k=-\infty}^{\infty} \sum_{j=0}^{N_f-1} \hat{x}_i[k]\, w_{tx}(t - jT_f - kT_s), \tag{2.10}$$

which is then re-transmitted to the next relay ($1 \leq i \leq m-2$) or the destination node ($i = m-1$). Here, α_{i+1} denotes the power allocation

[1] Similar to the filter bandwidth W, the integration duration T_i has to be optimized such that (on average) most of the signal energy is captured, while the collected noise energy is kept to a minimum.

factor for the ith relay node.

In the case of D&F relaying, a hard decision on the symbols $\hat{x}_i[k]$ would be performed prior to re-transmission, followed by a FEC decoding step. Note that D&F relaying is thus more complex than A&F relaying.

2.5 Proposed Structure of the Destination Node

The receiver structure of the destination node is identical to that of the relays. In particular, we assume an identical bandpass filter $h_{BP}(t)$ for simplicity. Similar to (2.6), the filtered received signal is given by

$$\begin{aligned} r_m(t) &= \sqrt{A_m}\,(h_m(t) * h_{BP}(t)) * s_m(t) + n_m(t) \\ &= \sqrt{A_m \alpha_m E_g} \sum_{k=-\infty}^{\infty} \sum_{j=0}^{N_f-1} \hat{x}_{m-1}[k]\, w_{rx,m}(t - jT_f - kT_s) + n_m(t), \end{aligned} \tag{2.11}$$

where $w_{rx,m}(t) := w_{tx}(t) * h_m(t) * h_{BP}(t)$ and $h_m(t)$ denotes the CIR of the final link (Link m). In order to recover the symbols $q_1[k]$ transmitted by the source node, the destination node performs another differential decoding step followed by an integrate-and-dump operation. This yields estimated symbols

$$\hat{x}_m[k] = \sum_{j=0}^{N_f} \int_{kT_s+jT_f}^{kT_s+jT_f+T_i} r_m(t) r_m(t - T_s) dt \tag{2.12}$$

(cf. Fig. 2.2 (c)), which are used for decoding of the transmitted information bits. At the destination node, the Viterbi algorithm is used for decoding the output of the integration-and-dump unit. We consider both hard and soft

input Viterbi decoding. In hard decoding, $\hat{x}_m[k]$ is passed through a slicer, in order to arrive at the hard estimates $\hat{q}_1[k]$ of the transmitted symbols $q_1[k]$. Subsequently, Viterbi decoding is performed based on $\hat{q}_1[k]$ ('FEC^{-1}'), in order to obtain estimates $\hat{b}[\kappa]$ for the transmitted information bits $b[\kappa]$. In contest, in the soft input Viterbi decoding, the soft estimates, $\hat{x}_m[k]$, are used to obtain estimates of the transmitted bits. The squared Euclidean distance is used as a metric for soft input Viterbi decoding. In Chapter 4, it will be shown that the input-output behavior of the system can be described as $\hat{x}_m[k] = \tilde{\beta}_m\, q_1[k] + z_m[k]$, where $\tilde{\beta}_m$ and $z_m[k]$ are a gain factor and a noise sample, respectively (c.f. Section 4.1). Thus, we use the following branch metric for the soft input Viterbi decoder [37]

$$\iota[k] = |\hat{x}_m[k] - \tilde{\beta}_m \tilde{q}_1[k]|^2, \tag{2.13}$$

where $\tilde{q}_1[k] \in \{\pm 1\}$ denotes a trial symbol.

Chapter 3

Dual-hop Case

In the following, we analyze the performance of dual-hop IR-UWB with double differential encoding at the source. In this case, we have only one relay i.e., $m = 2$. We show that the output of this system can be written in terms of the input as

$$\hat{x}_3[k] = \tilde{\beta}_3 \, q_1[k] + z_3[k], \tag{3.1}$$

where $\tilde{\beta}_3$ and $z_3[k]$ represent a gain factor and an effective noise sample, respectively. Note that $w_3[k]$ is in general non-Gaussian, so finding a closed-form expression for the BER seems difficult. Therefore, we focus on the effective SNR at the destination node in Section 3.1. In particular, a closed-form expression for the SNR at the destination node is derived. In Section 3.2, keeping the total power fixed, an optimum solution for power allocation factors α_1 and α_2 is devised to maximize the SNR at the destination. Based on the results of this section, we propose a method for optimization of the power allocation factors of more complex multi-hop systems in Chapter 4.

3.1 Effective SNR at the Destination Node for the Dual-Hop Case

We start by substituting the filtered received signal $r_1(t)$ at the relay, cf. (2.6) ($i=1$), into (2.8) and get

$$\hat{x}_1[k] = \beta_1 \overbrace{q_3[k]q_3[k-1]}^{=q_2[k]} + z_1[k], \tag{3.2}$$

where $\beta_1 := N_f A_1 \alpha_1 \varepsilon_1$, $\varepsilon_1 := E_g \int_0^{T_i} w_{rx,1}^2(t)dt$, and $z_1[k] := z'_{1,1}[k] + z'_{1,2} + z'_{1,3}[k]$ with $z'_{1,1}[k]$, $z'_{1,2}$, and $z'_{1,3}[k]$ being zero-mean noise terms defined as follows:

$$z'_{1,1}[k] := q_3[k]\sqrt{A_1\alpha_1 E_g} \sum_{j=0}^{N_f-1} \int_{kT_s+jT_f}^{kT_s+jT_f+T_i} n_1(t-T_s) w_{rx,1}(t-jT_f-kT_s)\, dt, \tag{3.3}$$

$$z'_{1,2}[k] := q_3[k-1]\sqrt{A_1\alpha_1 E_g} \sum_{j=0}^{N_f-1} \int_{kT_s+jT_f}^{kT_s+jT_f+T_i} n_1(t) w_{rx,1}\left(t-jT_f-kT_s\right) dt, \tag{3.4}$$

$$z'_{1,3}[k] := \sum_{j=0}^{N_f-1} \int_{kT_s+jT_f}^{kT_s+jT_f+T_i} n_1(t) n_1(t-T_s)\, dt. \tag{3.5}$$

As described earlier, $n_1(t)$ is obtained by filtering an AWGN process with single-sided noise PSD $\frac{N_0}{2}$ with a bandpass filter with one-sided bandwidth W. The autocorrelation function (ACF) $\phi_1(\tau)$ of $n_1(t)$ is thus given by [37]

$$\phi_1(\tau) = E\{n_1(t)n_1(t-\tau)\} = \frac{N_0}{2} \cdot \frac{\sin(\pi W\tau)}{\pi W\tau} \cos(2\pi f_0 \tau), \tag{3.6}$$

where f_0 denotes the center frequency of the bandpass filter, and $E\{\cdot\}$ denotes statistical expectation. Assuming that the bandwidth W is chosen sufficiently large, such that the frequency response of the received pulse $w_{rx,1}(t)$ falls completely inside the PSD $\Phi_1(f)$ of $n_1(t)$, and the PSD $\Phi_1(f)$ is sufficiently flat in the area of interest, the ACF $\phi_1(\tau)$ can be replaced by $\frac{N_0}{2}\,\delta(\tau)$. Thus, the variances of the noise terms $z'_{1,1}[k]$, $z'_{1,2}[k]$, and $z'_{1,3}[k]$ can be approximated as

$$\begin{aligned}
\sigma^2_{z'_{1,1}} &= E\{z'^2_{1,1}[k]\} = N_f A_1 \alpha_1 E_g \int_0^{T_i}\int_0^{T_i} w_{rx,1}(t) w_{rx,1}(\tau)\phi_1(t-\tau)dtd\tau \\
&\approx N_f A_1 \alpha_1 E_g \frac{N_0}{2}\int_0^{T_i} w^2_{rx,1}(t)dt = \beta_1 \frac{N_0}{2}, \qquad (3.7)\\
\sigma^2_{z'_{1,2}} &= E\{z'^2_{1,2}[k]\} = \sigma^2_{z'_{1,1}}, \qquad (3.8)\\
\sigma^2_{z'_{1,3}} &= E\{z'^2_{1,3}[k]\} = N_f \int_0^{T_i}\int_0^{T_i} \phi_1^2(t-\tau)dtd\tau = N_f \int_0^{T_i}\int_{T_i-t}^{T_i} \phi_1^2(u)dtdu,\\
&= N_f \int_0^{T_i} \frac{N_0^2}{4}\cdot 2\cdot W dt = \frac{W N_f T_i N_0^2}{2}. \qquad (3.9)
\end{aligned}$$

In (3.9), we have exploited the fact that the integrand $\phi_1^2(u)$ is Dirac-like, i.e., the integral vanishes outside $[-t, T_i - t]$, and we have employed Parseval's theorem to calculate the integral. Altogether, the variance of the noise term $z_1[k] = z'_{1,1}[k] + z'_{1,2} + z'_{1,3}[k]$ in (3.2) is given by $\sigma_1^2 := \beta_1 N_0 + \frac{W N_f T_i N_0^2}{2}$. Note that $z_1[k]$ is not Gaussian distributed, since $z'_{1,3}[k]$ is not Gaussian.

Along the same lines, the integrator output of the destination node can be analyzed. Substituting (2.11) into (2.12) ($i=1$, $m=2$) yields

$$\hat{x}_2[k] = \beta_2 \hat{x}_1[k]\hat{x}_1[k-1] + z'_2[k], \qquad (3.10)$$

where $\beta_2 := N_f A_2 \alpha_2 \varepsilon_2$, $\varepsilon_2 := E_g \int_0^{T_i} w_{rx,2}^2(t)dt$, and the noise term $z'_2[k] = z'_{2,1}[k] + z'_{2,2}[k] + z'_{2,3}[k]$ is similarly defined as in (3.2) and (3.3)–(3.5), with $q_3[k]$ being replaced by $\hat{x}_1[k]$, A_1 by A_2, α_1 by α_2, $n_1(t)$ by $n_2(t)$, and $w_{rx,1}(t)$ by $w_{rx,2}(t)$. Plugging $\hat{x}_1[k]$ from (3.2), into (3.10) we get

$$\hat{x}_2[k] = \beta_2\beta_1^2 \overbrace{q_2[k]q_2[k-1]}^{=q_1[k]} + z'_2[k] + z'_{2,4}[k] + z'_{2,5}[k] + z'_{2,6}[k], \tag{3.11}$$

where $z'_{2,4}[k]$, $z'_{2,5}[k]$, and $z'_{2,6}[k]$ are defined as

$$z'_{2,4}[k] = \beta_2\beta_1 q_2[k] z_1[k-1], \tag{3.12}$$

$$z'_{2,5}[k] = \beta_2\beta_1 q_2[k-1] z_1[k], \tag{3.13}$$

$$z'_{2,6}[k] = \beta_2 z_1[k] z_1[k-1]. \tag{3.14}$$

The variances of $z'_{2,1}[k]$, $z'_{2,2}[k]$, and $z'_{2,3}[k]$ can be calculated similarly to (3.7)–(3.9). One obtains

$$\begin{aligned} \sigma^2_{z'_{2,1}} &\approx E\{\hat{x}_1^2[k]\}\beta_2\frac{N_0}{2} = (\beta_1^2 + \sigma_1^2)\beta_2\frac{N_0}{2}, \\ & \sigma^2_{z'_{2,2}} = \sigma^2_{z'_{2,1}}, \quad \sigma^2_{z'_{2,3}} = \sigma^2_{z'_{1,3}}. \end{aligned} \tag{3.15}$$

The variances of $z'_{2,4}[k]$, $z'_{2,5}[k]$, and $z'_{2,6}[k]$ can be calculated from (3.12)–(3.14):

$$\sigma^2_{z'_{2,4}} = \sigma^2_{z'_{2,5}} = (\beta_2\beta_1)^2\sigma_1^2 \quad \text{and} \quad \sigma^2_{z'_{2,6}} \approx \beta_2^2\sigma_1^4. \tag{3.16}$$

For computing the variance of $z'_{2,6}[k]$, we have assumed that $z_1[k]$ and

$z_1[k-1]$ are statistically independent. Based on (3.11)–(3.16), we are now ready to obtain the input-output behavior of our system according to (3.1), where $\tilde{\beta}_2 := \beta_2\beta_1^2$ and $z_2[k] := z'_2[k]+z'_{2,4}[k]+z'_{2,5}[k]+z'_{2,6}[k]$. In order to calculate the variance of $z_2[k]$, denoted as σ_2^2 in the sequel, we note that $z'_{2,4}[k]$ and $z'_{2,5}[k]$ are not mutually independent, i.e., their correlation cannot be ignored. In particular, one finds that

$$\begin{aligned} E\{z'_{2,4}[k]z'_{2,5}[k]\} &= (\beta_2\beta_1)^2 E\{q_2[k]q_2[k-1]z_1[k]z_1[k-1]\} \\ &= (\beta_2\beta_1)^2 E\{q_2[k]q_2[k-1]z'_{1,1}[k]z'_{1,2}[k-1]\}. \end{aligned} \tag{3.17}$$

A careful look at (3.3)–(3.3) reveals that $q_3[k-2]z'_{1,2}[k-1] = q_3[k]z'_{1,1}[k]$. Thus, we have

$$\begin{aligned} E\{q_2[k]q_2[k-1]z'_{1,1}[k]z'_{1,2}[k-1]\} &= E\{q_3[k]q_3[k-2]z'_{1,1}[k]z'_{1,2}[k-1]\} \\ &= E\{z'^2_{1,1}[k]\} = \beta_1\frac{N_0}{2} \end{aligned} \tag{3.18}$$

and get

$$E\{z'_{2,4}[k]z'_{2,5}[k]\} = \beta_2^2\beta_1^3\frac{N_0}{2}. \tag{3.19}$$

Based on (3.1) and (3.11)–(3.19), the effective SNR at the destination node can be calculated as

$$\begin{aligned} \text{SNR} &= \frac{\tilde{\beta}_2^{\,2}}{\sigma_2^2} = \frac{(\beta_2\beta_1^2)^2}{\sigma^2_{z'_{2,4}} + \sigma^2_{z'_{2,5}} + \sigma^2_{z'_{2,6}} + 2E\{z'_{2,4}[k]z'_{2,5}[k]\} + \sigma^2_{z'_2}} \\ &\approx \frac{(\beta_2\beta_1^2)^2}{\beta_2^2\left(2\beta_1^2\sigma_1^2 + \beta_1^3N_0 + \sigma_1^4\right) + \beta_2N_0(\beta_1^2+\sigma_1^2) + \frac{WN_fT_iN_0^2}{2}}. \end{aligned} \tag{3.20}$$

3.2 Optimized Transmit Power Allocation for the Dual-Hop Case

Based on (3.20), we can now optimize the transmit power allocation factors α_1 and α_2 for the source node and the A&F relay, respectively. We aim to maximize the effective SNR at the destination node, under the constraint of keeping the total transmit power fixed.

It can be shown that the total transmit power constraint can be expressed as

$$\alpha_1 + \alpha_2(\beta_1^2 + \sigma_1^2) \stackrel{!}{=} 1. \tag{3.21}$$

Concerning (3.20), we can make a high-SNR approximation, according to

$$\text{SNR} \approx \frac{\beta_2\beta_1^2}{\beta_2(2\sigma_1^2 + \beta_1 N_0) + N_0}, \tag{3.22}$$

where we have used that, for high SNR values, $2\beta_1^2\sigma_1^2 + \beta_1^3 N_0 \gg \sigma_1^4$, $\beta_1^2 \gg \sigma_1^2$, and $\frac{WN_fT_iN_0^2}{2}$ becomes negligible.

Assuming again high SNR, we can now formulate the Lagrange problem

$$\Lambda(\alpha_1, \alpha_2, \gamma) = \frac{\beta_2\beta_1^2}{(3\beta_1\beta_2 + 1)N_0} - \gamma(\alpha_1 + \alpha_2\beta_1^2 - 1), \tag{3.23}$$

where γ denotes the Lagrange multiplier. In order to arrive at (3.23), we have used the high-SNR approximations $\beta_1^2 \gg \sigma_1^2$ and $\sigma_1^2 \approx \beta_1 N_0$. Based on (3.23), the optimal transmit power allocation results as

$$\alpha_{1,\text{opt}} = \frac{1}{1 + \sqrt{\frac{A_1}{3A_2}}}, \qquad \alpha_{2,\text{opt}} = \frac{1 - \alpha_{1,\text{opt}}}{\beta_1^2 + \sigma_1^2}, \tag{3.24}$$

which only depends on the link gains A_1 and A_2. The numerical results in Chapter 6 will reveal that (3.24) is, in fact, very close to the optimal solution (also for moderate SNR values).

Chapter 4

Multi-hop Case

In the following, we turn to the case of multiple hops ($m>2$). In particular, we derive a closed-form expression for the effective SNR at the destination node and use this expression for optimization of the power allocation factors for the source node and the A&F relays.

4.1 Effective SNR at the Destination Node for the Multi-Hop Case

Similar to (3.1), the input-output behavior of the system can be described as

$$\hat{x}_m[k] = \tilde{\beta}_m \, q_1[k] + z_m[k], \tag{4.1}$$

where $\tilde{\beta}_m$ and $z_m[k]$ represent a gain factor and an effective noise sample, respectively. We note again that $z_m[k]$ is in general non-Gaussian. In order to obtain an expression for the gain factor $\tilde{\beta}_m$, the noise term $z_m[k]$, and the corresponding noise variance σ_m^2 (and finally the effective SNR $\tilde{\beta}_m^2/\sigma_m^2$ at the destination node), the following recursion steps are required (similar to the derivation for the dual-hop case in Section 3.1):

- Assume that we have already obtained the input-output relation for

the soft estimate $\hat{x}_i[k]$ formed by the ith relay, according to

$$\hat{x}_i[k] = \beta_i q_{m-i+1}[k] + z_i[k] \tag{4.2}$$

$(i=1)$ or

$$\hat{x}_i[k] = \tilde{\beta}_i q_{m-i+1}[k] + z_i[k] \tag{4.3}$$

$(1 < i < m)$, cf. (3.1) and (3.2) for the dual-hop case. In particular, assume that we have calculated the gain factor β_i or $\tilde{\beta}_i$ and the variance σ_i^2 of the noise term $z_i[k]$. In the sequel, we focus on the case $i>1$ for simplicity. For $i=1$, parameter $\tilde{\beta}_i$ needs to be replaced by β_i in the following equations.

- For the integrator output of the $(i+1)$th relay $(i < m-1)$ or the destination node $(i=m-1)$, we obtain the relation

$$\hat{x}_{i+1}[k] = \beta_{i+1}\hat{x}_i[k]\hat{x}_i[k-1] + z'_{i+1}[k], \tag{4.4}$$

where $\beta_{i+1} := N_f A_{i+1}\alpha_{i+1}\varepsilon_{i+1}$, $\varepsilon_{i+1} := E_g \int_0^{T_i} w_{rx,i+1}^2(t)dt$, and $z'_{i+1}[k]$ represents a zero-mean noise term with components defined similar to (3.3–3.5), with $q_3[k]$ being replaced by $\hat{x}_i[k]$, A_1 by A_{i+1}, α_1 by α_{i+1}, $n_1(t)$ by $n_{i+1}(t)$, and $w_{rx,1}(t)$ by $w_{rx,i+1}(t)$. The variance of the noise term $z'_{i+1}[k]$ is calculated[2] as $\sigma^2_{z'_{i+1}} \approx (\tilde{\beta}_i^2 + \sigma_i^2)\beta_{i+1}N_0 + \frac{WT_iN_0^2}{2}$.

- Plugging the expression for $\hat{x}_i[k]$ from (4.3) into (4.4), we obtain a new

[2]Derivation is described in Appendix A.1

representation for the soft estimate $\hat{x}_{i+1}[k]$, according to

$$\hat{x}_{i+1}[k] = \tilde{\beta}_{i+1} q_{m-i}[k] + z_{i+1}[k]. \tag{4.5}$$

The gain factor $\tilde{\beta}_{i+1}$ is obtained via the recursion

$$\tilde{\beta}_{i+1} = \beta_{i+1}\tilde{\beta}_i^2. \tag{4.6}$$

Moreover, making similar approximations as in Section 3.1 and taking the correlations between the involved noise terms into account, the variance σ_{i+1}^2 of the noise term $z_{i+1}[k]$ can be calculated[3] via the recursion

$$\sigma_{i+1}^2 \approx \beta_{i+1}^2 \left(2\tilde{\beta}_i^2(\sigma_i^2 + \eta_i) + \sigma_i^4\right) + \beta_{i+1} N_0(\tilde{\beta}_i^2 + \sigma_i^2) + \frac{W N_f T_i N_0^2}{2}, \tag{4.7}$$

where

$$\eta_i \approx \beta_i^2 \tilde{\beta}_{i-1}^2 \left(\sigma_{i-1}^2 + 2\eta_{i-1}\right) + \beta_{i-1}\tilde{\beta}_{i-1}^2 \frac{N_0}{2}. \tag{4.8}$$

Here, we have used the approximation that for a small to moderate number of intermediate A&F relays the correlation between the noise terms $z'_{i+1}[k]$ and $z_{i+1}[k]$, cf. (4.4) and (4.5), can be neglected.

[3] Calculation is explained in Appendix A.2 with more details

At the end of the recursion ($i = m$–1), we thus obtain the following expression for the effective SNR at the destination node:

$$\begin{aligned} \text{SNR} &= \frac{\tilde{\beta}_m^2}{\sigma_m^2} \\ &\approx \frac{(\beta_m \tilde{\beta}_{m-1}^2)^2}{\beta_m^2 \left(2\tilde{\beta}_{m-1}^2(\sigma_{m-1}^2 + \eta_{m-1}) + \sigma_{m-1}^4\right) + \beta_m N_0(\tilde{\beta}_{m-1}^2 + \sigma_{m-1}^2) + \frac{W N_f T_i N_0^2}{2}} \,. \end{aligned} \tag{4.9}$$

Based on the above results, in the following, we will propose an algorithm for obtaining a suboptimal, yet efficient solution for the transmit power allocation factors α_i for the source node ($i = 1$) and the relay nodes ($2 \leq i \leq m$), with the goal to maximize the effective SNR at the destination node.

4.2 Optimized Transmit Power Allocation for the Multi-Hop Case

A closed-form solution for the optimal transmit power allocation factors α_i ($1 \leq i \leq m$) does not seem feasible in the multi-hop case ($m > 2$) because of the involved expression for the SNR (4.9). Thus, in the following, we present a heuristic algorithm for finding near-optimal values for the transmit power allocation factors α_i. The proposed algorithm is based on the optimization presented in Section 3.2 for the dual-hop case. Essentially, we decompose the m–hop transmission into $m - 1$ two-hop transmissions. In particular, we first assume that there are only three nodes, namely the source node, the last relay ($i = m$), and the destination node and find the corresponding

optimal transmit power factor for the source-relay link. In the next step, the transmit power allocated to the source node in the previous step is regarded as the overall available transmit power, and the optimum power allocation between the source node and the $(m-2)$th relay (Node $m-1$) is calculated assuming that the $(m-1)$th relay (Node m) is the destination. We apply this method repeatedly until we find the overall power allocation for the source node and subsequently calculate the powers allocated to each relay in a similar manner.

In the following, let $A_{i,j}$ denote the gain factor associated with the link from node i to node j, cf. (2.5) and Fig. 4.1, where $i = 1$ represents the source node and $j = m+1$ the destination node. Assuming we have only the source (Node 1), the last relay (Node m), and the destination (Node $m+1$), according to (3.24), the power factor for the source, ζ_m^1, is given by

$$\zeta_m^1 = \frac{1}{1 + \sqrt{\frac{A_{1,m}}{3A_{m,m+1}}}}. \tag{4.10}$$

The fraction of power allocated to the $(m-1)$th relay (Node m) is given by $1 - \zeta_m^1$. However, we cannot calculate the associated power allocation factor α_m since the received power of the relay is not known yet. Instead, in the next step, we consider $N_f E_g \zeta_m^1$ to be the available power and take into account that the received signal at the $(m-1)$th relay (Node m) actually originates from the $(m-1)$th relay. To find the corresponding power allocation, we consider only the source, relay $i = m-1$, and relay $i = m$, with the latter playing the role of the destination. Therefore, the fraction of power allocated to the source is now given by $\zeta_m^1 \zeta_{m-1}^1$. This procedure is

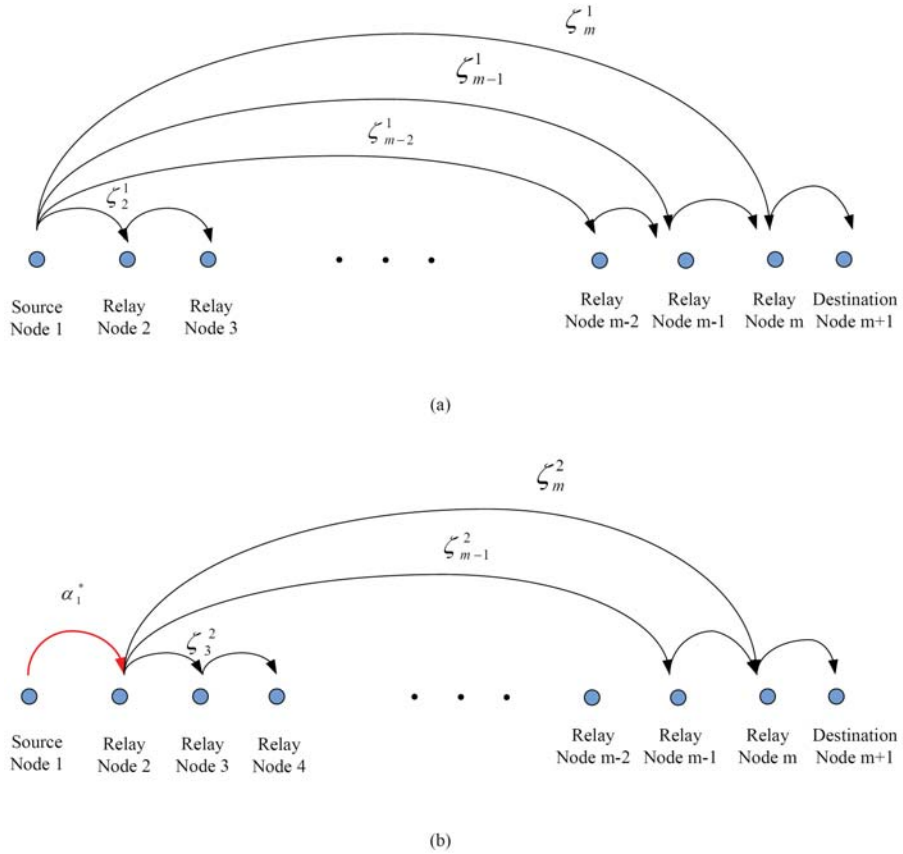

Figure 4.1: (a) Optimizing α_1^* using a recursive approach. (b) Optimization of α_2^* for known α_1^*.

repeated until we arrive at first relay ($i = 2$) , which leads to the following final power allocation for the source:

$$\alpha_1^* = \prod_{i=2}^{m} \zeta_i^1 \tag{4.11}$$

At each step we will have the following expression for the fraction of

power allocated to each link

$$\zeta_i^1 = \frac{1}{1+\sqrt{\frac{1}{3}\cdot\frac{A_{1,i}}{A_{i,i+1}}}}. \tag{4.12}$$

Knowing the power allocated to the source, the available power for allocation to the $m-1$ relays is given by $(1-\alpha_1^*)N_f E_g$. The power allocation factor for relay 1 is constrained by

$$\alpha_2 E_{rx,1} + \bar{E}_2 = 1 - \alpha_1^*, \tag{4.13}$$

where $E_{rx,1} := \beta_1^2 + \sigma_1^2$ denotes the received power of first relay and $\bar{E}_2$ is the remaining power to be allocated to the other $m-2$ relays later on. The power allocation factor α_2 of the first relay ($i=2$) is now obtained using the same recursive approach as for the source before, i.e., the first relay plays the role of the source. Subsequently, the same steps are repeated for relays $i=3$ to $i=m$. For the jth relay, $1 \leq j \leq m-1$, this leads to power allocation

$$\alpha_{j+1}^* = \frac{\kappa_j}{E_{rx,j}} \cdot \prod_{i=j+2}^{m} \zeta_i^{j+1}, \tag{4.14}$$

with

$$\zeta_i^j = \frac{1}{1+\sqrt{\frac{A_{j,i}}{3A_{i,i+1}}}}. \tag{4.15}$$

$$\kappa_j = \kappa_{j-1} - \alpha_j^* E_{rx,j-1} \tag{4.16}$$

$$E_{rx,j} = (A_j \alpha_i E_{rx,j-1} N_f E_j)^2 + \sigma_j^2 \tag{4.17}$$

where the received power at ith relay, $E_{rx,i}$, and normalization factor κ_i, are calculated recursively for $i \geq 2$. For initialization, we have $\kappa_0 := 1$ and $E_{rx,0} = 1$. It is easy to check that the suboptimal power allocation in (4.14) fulfills the overall power constraint $N_f E_g \alpha_1^* + \sum_{i=2}^{m} \alpha_i^* N_f E_g E_{rx,i-1} = N_f E_g$.

Although the proposed heuristic power allocation scheme for the multi-hop case is suboptimal, our results in Chapter 6 will confirm its near-optimal performance. Furthermore, the proposed power allocation algorithm allows for a semi-distributed implementation, where the source has to have only access to estimates of its own path loss to all relays and the path-losses between all neighboring relays. In particular, for the proposed semi-distributed implementation, the source computes the factors $f_j := \prod_{i=j}^{m} \zeta_i^j$, $1 \leq j \leq m$, feeds back f_{j+1} to jth relay, computes α_1^*, and feeds back $\kappa_1 = 1 - \alpha_1^*$ to first relay. The jth relay, $1 \leq j \leq m-1$, estimates its own received power $E_{rx,j}$, computes α_j^* based on (4.14), computes κ_j based on (4.16), and feeds back κ_j to the next $(j+1)$th relay. The last relay only has to estimate $E_{rx,m-1}$ and compute α_m^*.

Chapter 5

Performance Analysis of Dual-hop Transmission with Rake Receiver

In Chapter 6, the performance of the proposed scheme is compared with a Rake receiver for dual-hop relaying. To have a fair comparison between Rake receivers and differential receivers, the power allocation factors for Rake reception should be optimized for maximization of the SNR at the destination. So here, we first describe the model of the Rake receiver and then calculate the SNR of the destination for Rake reception at the relay and the destination, respectively. Then, based on the expression for the SNR, the power allocation factors are optimized for dual-hop transmission.

5.1 Effective SNR at the Destination Node

The performance of a pulse based Rake receiver has been studied in [13]. Here, we want to give a brief overview of the analytical basis for Rake receiver systems. In Rake combiners, the received signal is correlated with an

appropriate template signal which is designed to capture energy of the signal efficiently. The output of the correlator is passed through an integration-and-dump block. The output of the integration-and-dump unit is either transmitted to the next node (in A&F relay) or used for decision making (in D&F relay or destination node).

The transmitted signal at the source can be described as

$$s_1(t) = \sqrt{\alpha_1 E_g} \sum_{k=-\infty}^{\infty} \sum_{j=0}^{N_f-1} b[k]\, w_{tx}(t - jT_f - kT_s), \tag{5.1}$$

where $b[k] \in \{\pm 1\}$ denotes the information bit, α_1 is the power allocation factor for the transmitter, and E_g represents the energy per pulse. $w_{tx}(t)$ is the transmited pulse shape with duration T_p such that $\int_0^{T_p} w_{tx}^2(t)dt = 1$, as before.

As described earlier, the multipath model of channel model is defined based on [34] as (2.2)

$$h_r(t) = \sum_{\nu=0}^{L_C} \sum_{\mu=0}^{L_R} \lambda_{\mu,\nu}^{(r)}\, \delta(t - T_\nu^{(r)} - \tau_{\mu,\nu}^{(r)}). \tag{5.2}$$

To simplify our analysis, for performance evaluation, it is assumed that the multipath arrival times are multiples of the minimum resolvable path interval, T_p. Thus, we can rewrite the channel model as

$$h_r(t) = \sum_{l=1}^{L} \lambda_l^{(r)} \delta(t - (l-1)T_p). \tag{5.3}$$

If there is no arrival at an specific time ($(k-1)T_p$), the corresponding channel

coefficient gain will be zero ($\lambda_k^{(r)} = 0$).

The received signal at the relay is the convolution of the transmitted signal with the CIR and described by

$$r_1(t) = \sqrt{\alpha_1 A_1 E_g} \sum_{k=-\infty}^{\infty} \sum_{j=0}^{N_f-1} b[k] w_{rx}^{(1)}(t - jT_f - kT_s) + n_R(t), \tag{5.4}$$

where $n_R(t)$ is zero-mean white Gaussian noise with variance Ω_n^2 and A_1 is the channel's relative gain which is given in (2.5) and $w_{rx}^{(1)}(t)$ is defined as [13]

$$w_{rx}^{(1)}(t) = \sum_{l=1}^{L} \lambda_l^{(1)} w_{tx}(t - (l-1)T_p). \tag{5.5}$$

Assuming a Rake receiver at the relay, a template signal is used for capturing and combining the energy of the received signal. The template signal is defined as

$$s_{\text{temp},k}(t) = \sum_{j=0}^{N_f-1} \vartheta(t - jT_f - kT_s), \tag{5.6}$$

where

$$\vartheta(t) = \sum_{l=1}^{L} \upsilon_l w_{tx}(t - (l-1)T_p), \tag{5.7}$$

and $\upsilon = [\upsilon_1, \ldots, \upsilon_l]$ are the weights for Rake combining. An S-Rake scheme is used in our analysis where the L_s most significant multi-path components are captured, causing only these components to be non-zero. There are different schemes for combining the signal components available in the literature, e.g. Equal Gain Combining (EGC) and Maximum Ratio Combining

(MRC) [38]. In EGC all the combining weights are equal, and they have the same weight in contributing to the final energy of the signal. However, in MRC we choose the Rake combining weights equal to the corresponding multipath coefficients i.e., for the ith realization of the channel, $\upsilon_l = \lambda_l^{(i)}$.

At the Rake receiver, the correlation between the received signal and the template signal is calculated. The output of the Rake receiver can be obtained as

$$y_1[k] = \sum_{j=0}^{N_f-1} \int_{kT_s+jT_f}^{kT_s+jT_f+T_i} r(t) s_{\text{temp},k}(t) dt. \tag{5.8}$$

Replacing (5.4) in (5.8), $y_1[k]$ can be rewritten as follows

$$\begin{aligned} y_1[k] = \sum_{j=0}^{N_f-1} \int_{kT_s+jT_f}^{kT_s+jT_f+T_i} & \left(\sqrt{\alpha_1 A_1 E_g} \sum_{k=-\infty}^{\infty} \sum_{n=0}^{N_f-1} b[k] w_{rx}^{(1)}(t - nT_f - kT_s) + n_R(t) \right) \\ & \times \left(\sum_{i=0}^{N_f-1} \sum_{l=1}^{L} \upsilon_l w_{tx}(t - (l-1)T_p - iT_f) \right) dt \\ = \sqrt{\alpha_1 A_1 E_g} \sum_{j=0}^{N_f-1} \int_{kT_s+jT_f}^{kT_s+jT_f+T_i} & \sum_{i=(k-1)T_s}^{kT_s} \sum_{l=1}^{L} \upsilon_l w_{tx}(t - (l-1)T_p - iT_f) \\ \times \left(\sum_{k=-\infty}^{\infty} \sum_{j=0}^{N_f-1} \sum_{r=1}^{L} \lambda_r^{(1)} w_{tx}(t - (r-1)T_p - jT_f - kT_s) + n_R(t) \right) & dt. \end{aligned} \tag{5.9}$$

Knowing that the duration of $w_{tx}(t)$ is T_p, (5.9) can be simplified to

$$y_1[k] = b[k] \sqrt{\alpha_1 A_1 E_1} \sum_{l=1}^{L} \lambda_l^{(1)} \upsilon_l + \hat{a} + n_{R,1}[k], \tag{5.10}$$

where $\hat{a}$ is an IFI term[4] and $E_1 = E_g(N_f \int_0^{T_i} w_{tx}^2(t)dt)^2$. The noise term, $n_{R,1}[k]$, is given by $n_{R,1}[k] := \sum_{j=0}^{N_f-1} \int_{kT_s+jT_f}^{kT_s+jT_f+T_i} n_R(t) s_{\text{temp},k}(t)dt$. Here we assume that $LT_p < T_f$ so there is no IFI (the assumption was made for the differential receiver). Therefore (5.10) can be rewritten as

$$y_1[k] = b[k]\sqrt{\alpha_1 A_1 E_1} \sum_{l=1}^{L} \lambda_l^{(1)} \upsilon_l + n_{R,1}[k], \tag{5.11}$$

where $n_{R,1}[k]$ is AWGN with zero mean. The variance of $n_{R,1}[k]$ can be calculated as

$$\begin{aligned}
\Omega_1^2 = E\{n_{R,1}^2[k]\} &= E\left\{ \left(\sum_{j=0}^{N_f-1} \int_{kT_s+jT_f}^{kT_s+jT_f+T_i} n_R(t) s_{\text{temp},k}(t)dt \right)^2 \right\} \\
&= E\left\{ \left(\sum_{j=0}^{N_f-1} \int_{kT_s+jT_f}^{kT_s+jT_f+T_i} \sum_{j=kN_f}^{(k+1)N_f-1} \sum_{l=1}^{L} n_R(t) \upsilon_l w_{tx}(t - jT_f - (l-1)T_p)dt \right)^2 \right\} \\
&= N_f \Omega_n^2 \sum_{l=1}^{L} \upsilon_l^2.
\end{aligned} \tag{5.12}$$

Relay retransmits $y_1[k]$ toward the destination. The transmitted signal from the relay can be expressed in a similar way as (5.1) as

$$s_2(t) = \sqrt{\alpha_2 E_g} \sum_{k=-\infty}^{\infty} \sum_{j=0}^{N_f-1} y_1[k]\, w_{tx}(t - jT_f - kT_s). \tag{5.13}$$

The received signal at the second Rake receiver is the convolution of $s_2(t)$ with the CIR of the second link plus additive white Gaussian noise, $n_{R'}(t)$, with the same statistical properties as $n_R(t)$. The output of second

[4]Performance analysis for the general case, including the case $LT_p > T_s$, can be found in [39].

Rake combiner can be derived along the same lines as (5.8)-(5.11). Finally, at the destination, we have

$$\begin{aligned} y_2[k] &= y_1[k]\sqrt{\alpha_2 A_2 E_2}\sum_{l=1}^{L}\lambda_l^{(2)}\upsilon_l + n_{R,2}[k], \\ &= b[k]\sqrt{\alpha_2 A_2 E_2}\sum_{l=1}^{L}\lambda_l^{(1)}\upsilon_l \cdot \sqrt{\alpha_1 A_1 E_1}\sum_{l=1}^{L}\lambda_l^{(2)}\upsilon_l \\ &\quad + n_{R,1}[k]\sqrt{\alpha_1 A_1 E_1}\sum_{l=1}^{L}\lambda_l^{(2)}\upsilon_l + n_{R,2}[k], \end{aligned} \tag{5.14}$$

where $E_2 = E_g(N_f \int_0^{T_i} w_{tx}^2(t)dt)^2$ and $n_{R,2}[k]$ is defined as follows

$$n_{R,2}[k] := \sum_{j=0}^{N_f-1}\int_{kT_s+jT_f}^{kT_s+jT_f+T_i} n'_R(t)s_{\text{temp},k}(t)dt. \tag{5.15}$$

The variance of $n_{R,2}[k]$ can be calculated with the same approach used for obtaining (5.12), which yeilds $\Omega_2^2 = E\{n_{R,2}^2[k]\} = N_f\Omega_n^2\sum_{l=1}^{L}\upsilon_l^2$. The total noise at destination, $n_{R,3}[k]$ is the sum of two noise terms,

$$n_{R,3}[k] = n_{R,1}[k]\sqrt{\alpha_1 A_1 E_1}\sum_{l=1}^{L}\lambda_l^{(2)}\upsilon_l + n_{R,2}[k]. \tag{5.16}$$

The variance of the noise at the destination can be calculated as follows

$$\Omega_3^2 = E\{n_3^2[k]\} = \alpha_2 A_2 E_2\Omega_2^2 + \Omega_1^2. \tag{5.17}$$

Splitting (5.14) into a signal part and a noise part, the SNR at the destina-

tion can be derived as

$$\mathrm{SNR} = \frac{\alpha_2 A_2 E_2 \cdot \alpha_1 A_1 E_1 (\sum_{l=1}^{L} \lambda_l^{(2)} \upsilon_l)^2 (\sum_{l=1}^{L} \lambda_l^{(1)} \upsilon_l)^2}{\frac{N_0}{2} \sum_{l=1}^{L} \upsilon_l^2 \ \left(1 + \alpha_2 A_2 E_2 (\sum_{l=1}^{L} \lambda_l^{(2)} \upsilon_l)^2\right)}. \tag{5.18}$$

5.2 Optimized Transmit Power Allocation

Based on (5.18), we can optimize the power allocation factors for the source-relay and relay-destination links. Here, the effective SNR at the destination node is optimized, under the constraint of keeping the total transmit power fixed. It can be shown that the total transmit power constraint can be expressed as

$$\alpha_1 + \alpha_2 \left(\alpha_1 A_1 E_1 \left(\sum_{l=1}^{L} \lambda_l^{(1)} \upsilon_l \right)^2 + \frac{N_0}{2} \sum_{l=1}^{L} \upsilon_l^2 \right) = 1. \tag{5.19}$$

To simplify our analysis, three variables are introduced as follows

$$\begin{aligned} K_1 &:= A_1 E_1 \left(\sum_{l=1}^{L} \lambda_l^{(1)} \upsilon_l \right)^2, \\ K_2 &:= A_2 E_2 \left(\sum_{l=1}^{L} \lambda_l^{(2)} \upsilon_l \right)^2, \\ K_3 &:= \frac{N_0}{2} \sum_{l=1}^{L} \upsilon_l^2. \end{aligned} \tag{5.20}$$

Using these variables, the power constraint can be re-written as

$$\alpha_1 + \alpha_2(\alpha_1 K_1 + K_3) = 1, \tag{5.21}$$

and the SNR simplifies to

$$\mathrm{SNR} = \frac{\alpha_1 \alpha_2 K_1 K_2}{K_3(1 + \alpha_2 K_2)}. \tag{5.22}$$

Based on (5.21) and (5.22), a Lagrange problem can be formulated. Using Lagrange multipliers, power allocation factors, α_1 and α_2 are optimized for maximization of the SNR at destination. Based on this approach, the result for the optimal power factor, $\alpha_{1,\mathrm{opt}}$, is as follows

$$\alpha_{1,\mathrm{opt}} = \frac{\sqrt{(K_1 + K_3)(K_2 + K_3)} - (K_2 + K_3)}{K_1 - K_2}. \tag{5.23}$$

For high SNR, K_3 is negligible compared to K_1 and K_2 because K_3 is a noise term and K_1 and K_2 are signal terms. So, assuming high SNR, (5.23) yields

$$\alpha_{1,\mathrm{opt}} \approx \frac{\sqrt{\frac{K_1}{K_2}} - 1}{\frac{K_1}{K_2} - 1} = \frac{1}{1 + \sqrt{\frac{K_1}{K_2}}}, \tag{5.24}$$

and α_2 can be calculated from (5.19) as

$$\alpha_{2,\mathrm{opt}} \approx \frac{1 - \alpha_{1,\mathrm{opt}}}{\alpha_{1,\mathrm{opt}} K_1 + K_3}. \tag{5.25}$$

If the CIRs of the first and the second links are similar, $\frac{K_1}{K_2} \approx \frac{A_1}{A_2}$ follows. So the optimal power allocation factor for the source is $\alpha_{1,\mathrm{opt}} \approx \frac{1}{1+\sqrt{\frac{A_1}{A_2}}}$, which only depends on the link gains A_1 and A_2 (similar to the DF case cf. (3.24)).

Since the comparison between Rake and DF receivers is made for the

dual-hop case in Chapter 6, we only consider the power allocation for this case here. However, extending our analysis to the multi-hop case is possible by following the same steps as in Chapter 4.

Chapter 6

Numerical Performance Results

In the following, we present numerical performance results, which illustrate the excellent performance of our proposed scheme and corroborate our analysis in Chapters 3 and 4. We start with considering the dual-hop case without channel coding. Afterwards, we present results for the multi-hop case and consider the benefits of an outer FEC scheme.

In the following, the information symbols $q_1[k] \in \{\pm 1\}$ are transmitted in blocks of 1000 symbols. The CIR is assumed to remain static for the duration of an entire block ($70\,\mu s$). As an example, we focus on channel model CM1 in the sequel and assume a path-loss exponent of $p = 3$ unless stated otherwise. One frame is used for transmitting a single information symbol ($N_f = 1$), and the frame length is chosen such that the guard interval between subsequent pulses is larger than the root-mean-square (rms) delay spread of the channel ($T_f = 70\,ns$), so as to circumvent ISI effects. For the transmitted pulse $w_{tx}(t)$, we employ the widely used second derivative of a

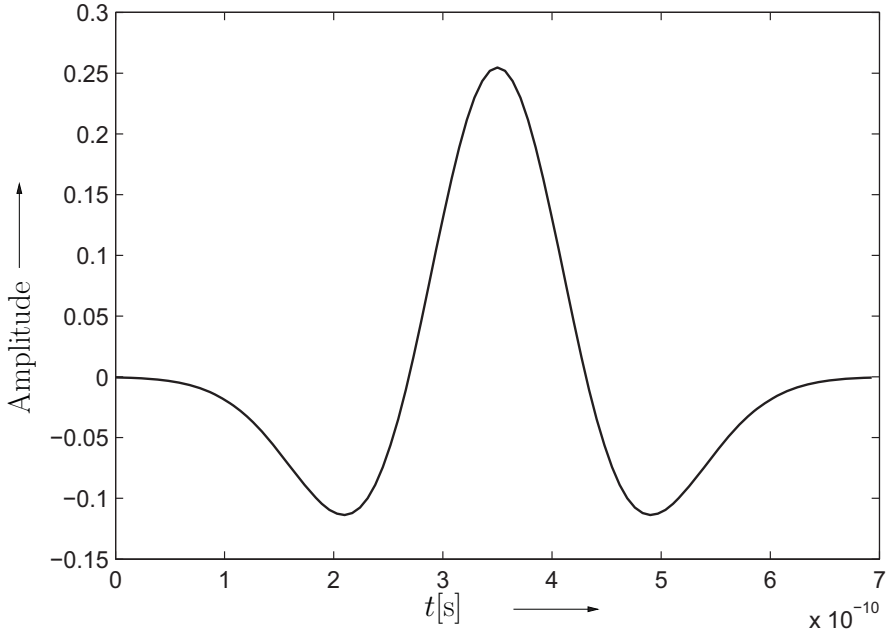

Figure 6.1: Transmitted pulse, $w_{tx}(t)$, in time domain.

Gaussian pulse, i.e.,

$$w_{tx}(t) = [1 - 4\pi(t - v_p)/v_m^2] \exp[-2\pi((t - v_p)/v_m)^2],$$

where $v_p = 0.35\,ns$ and $v_m = 0.2877\,ns$ ($T_p = 0.7\,ns$). Fig 6.1 shows the employed transmitted pulse in time domain.

The integration time T_i has been optimized such that on average the maximum effective SNR at the integrator output is obtained ($T_i = 5.25\,ns$). Moreover, the bandwidth W of the bandpass filter is optimized such that the maximum received SNR is obtained ($W = 5$ GHz). Fig. 6.2 depicts the frequency response of the transmitted pulse.

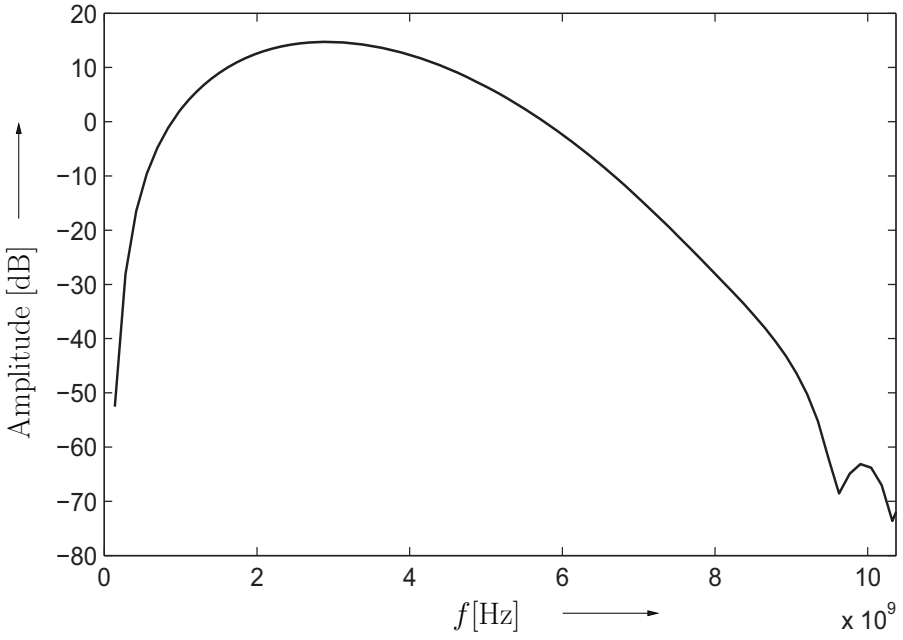

Figure 6.2: Transmitted pulse in frequency domain, $20\log(|w_{tx}(f)|)$.

Fig. 6.3 shows the effective SNR at the destination node for the double-differential A&F-relaying scheme for $E_g/N_0 = 9$ dB, considering three different positions of the relay ($\rho := d_1/d_{S-D} = \{0.2, 0.4, 0.8\}$), where d_1 and d_{S-D} denote the lengths of the source-relay and the source-destination link, respectively. Analytical results based on (3.20) are represented by lines, and corresponding simulation results are represented by markers. Moreover, the cross signs indicate the optimum value for the transmit power allocation factor α_1 for the source node, which was found based on (3.24). As can be seen, the analytical and the simulation results fit well, and considering the fact that our (approximate) formula (3.24) was derived for high SNR values

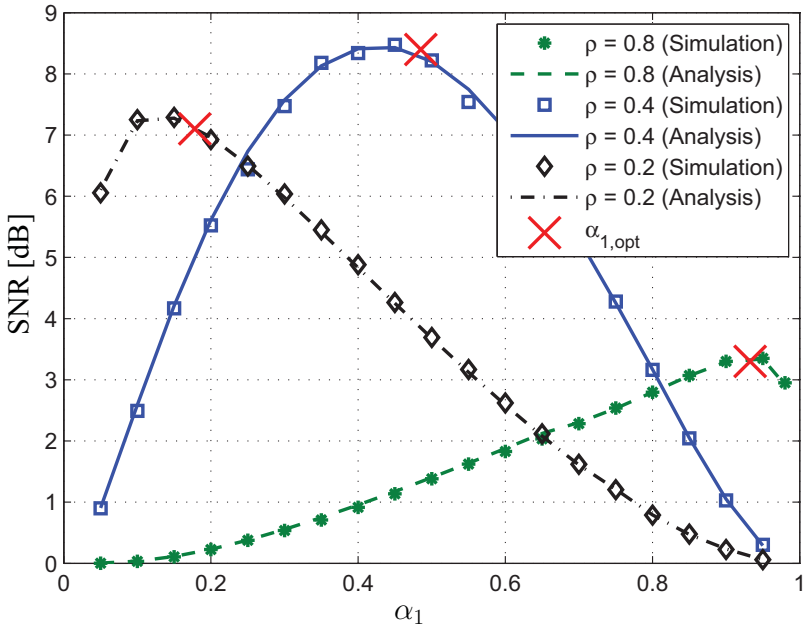

Figure 6.3: SNR at the destination versus α_1 for three different values for the source-relay distances and the optimal value of α_1 for each distance.

while the SNR considered in Fig. 6.3 is rather moderate, the optimal power allocation factor $\alpha_{1,\text{opt}}$ obtained with (3.24) offers a remarkable accuracy.

Fig. 6.4 illustrates the performance of the proposed non-coherent A&F relaying scheme with double-differential encoding at the source node, obtained by means of Monte-Carlo simulations over a large number of independent CIR realizations for $\rho = 0.2$. The proposed scheme is compared with (i) direct transmission from the source to the destination node, (ii) non-coherent A&F relaying with single differential encoding at the source node, (iii) coherent A&F and D&F relaying with S-Rake combining at the relay and at the destination node (using $L = 3, 5$ Rake-fingers), and (iv)

non-coherent D&F relaying scheme with double-differential encoding at the source node. The transmit power allocation factors α_1 and α_2 were optimized based on (3.24) for the proposed A&F relaying scheme with double-differential encoding and based on (5.24) for the A&F relaying scheme with Rake reception. For the other relaying schemes, power allocation factors are optimized based on simulations. As can be seen, all considered schemes offer substantial performance improvements over direct transmission. For sufficiently high SNR values, our proposed scheme outperforms the coherent A&F and D&F relaying schemes, unless a relatively large number of Rake fingers is employed (e.g., $L \geq 5$). The double-differential D&F relaying scheme offers a small performance advantage of about 0.5 dB compared to the A&F version, at the expense of an increased relay complexity. A&F relaying with straightforward single-differential encoding at the source, amplification at the relay, and differential decoding at the destination suffers from a significant loss in performance compared to the proposed scheme. We have doubled the integration time T_i at the receiver for A&F relaying with single-differential encoding since the effective CIR seen by the receiver is the convolution of the CIRs of the source-relay and the relay-destination channels. We note that the performance of A&F relaying with single-differential encoding could be improved by increasing the frame duration T_f at the expense of a loss in data rate.

Now, we consider the case when an outer FEC scheme is used. The FEC block is placed before the differential encoder and includes a convolutional encoder and a bit interleaver. The data is encoded with a 64-state, rate 1/2 binary convolutional code based on octal generators [133, 171] [37]. Fig. 6.5

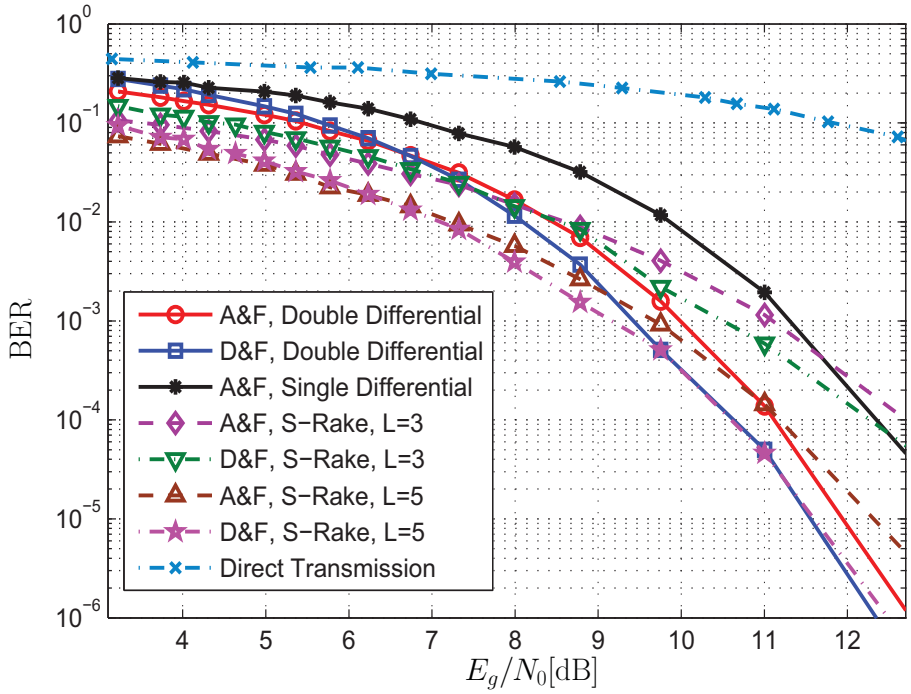

Figure 6.4: BER at the destination versus E_g/N_0 for double differential transmission and Rake receivers, respectively. A&F and D&F protocols.

shows the performance of the proposed non-coherent dual-hop A&F relaying scheme with double-differential encoding at the source node if an outer FEC scheme and hard input Viterbi decoding are used. As can be seen, using FEC improves the performance of all schemes significantly, especially that of the proposed scheme such that we can achieve BER in order of 10^{-5} for less than 8 dB. Similar to Fig. 6.4, we observe also in Fig. 6.5 that the performance of the Rake receiver is better than that of double-differentially transmission with A&F relaying only for lower SNRs.

Fig. 6.6 shows the performance of the proposed scheme if a soft input

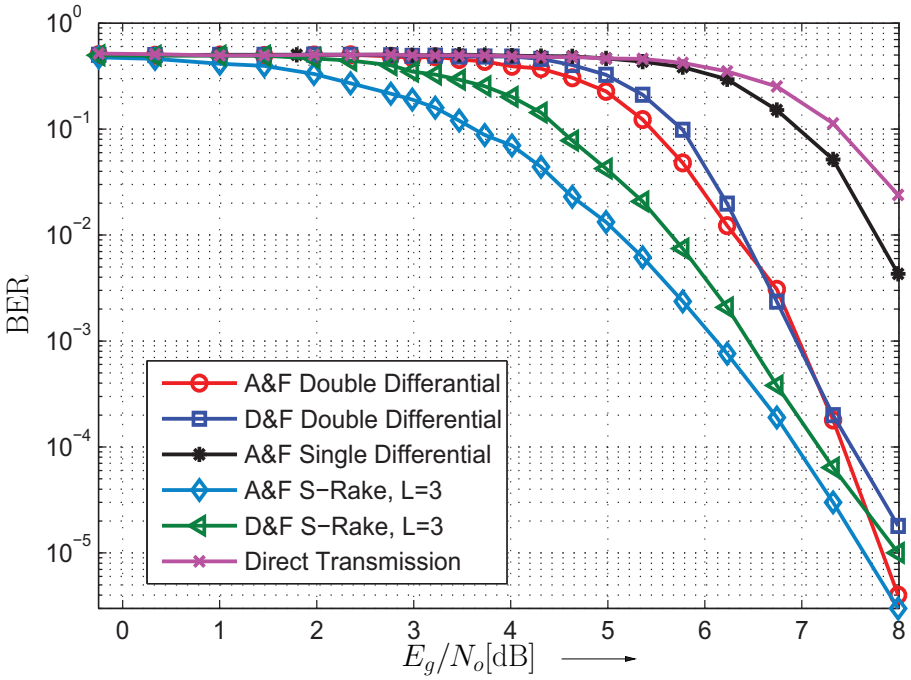

Figure 6.5: BER at destination versus E_g/N_0 for double differential encoding and Rake receivers with both A&F and D&F protocols in coded case (hard input Viterbi decoding).

Viterbi decoder is used at the destination. As can be seen, using soft decision decoding, the performance of the proposed non-coherent dual-hop A&F relaying scheme with double-differential encoding at the source node improves by more than 1 dB at the BER of 10^{-5}. Also the performance of other schemes improves significantly compared to hard decoding. Similar to Fig. 6.5, the slope of the curves in Fig. 6.6 suggest that the proposed scheme out performs coherent transmission with Rake receivers at high enough SNR. We note that Viterby decoding with squared Euclidean distance branch metric

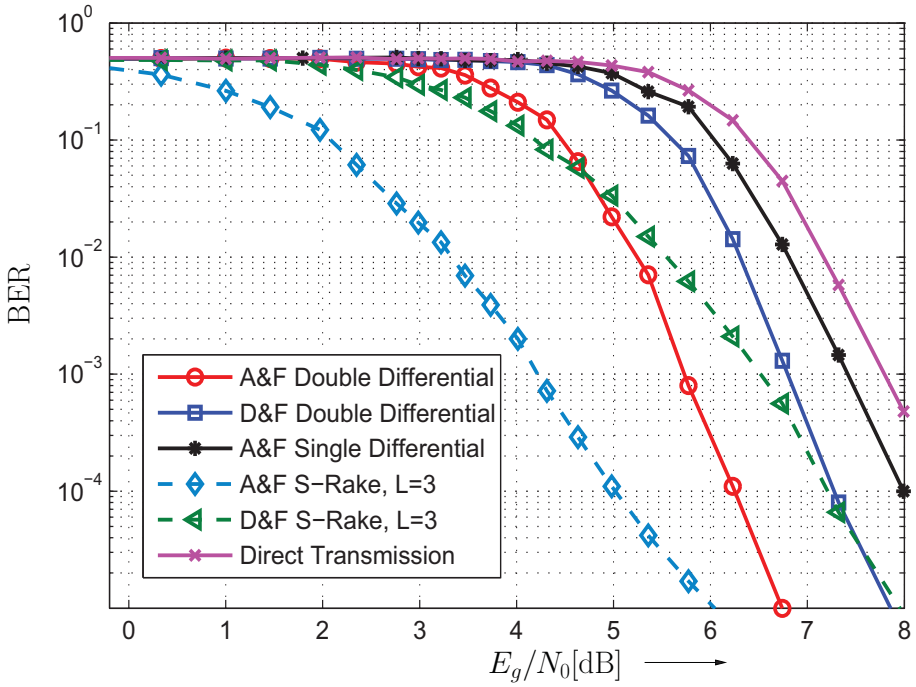

Figure 6.6: BER at destination versus E_g/N_0 for double differential encoding and Rake receivers with both A&F and D&F protocols in coded case (soft input Viterbi decoding).

is not necessary optimal for the proposed double-differential encoding since that the noise at the destination is non-Gaussian. As can be seen in Fig. 6.6, for the case of double differential encoding, the A&F scheme has a significantly better performance than the D&F scheme in the presence of soft input Viterbi decoding. This occurs because of the unreliable decision at the relay in D&F relaying which make the squared Euclidean distance metric staying suboptimal.

Fig. 6.7 depicts the BER versus ρ for a dual-hop IR-UWB system with

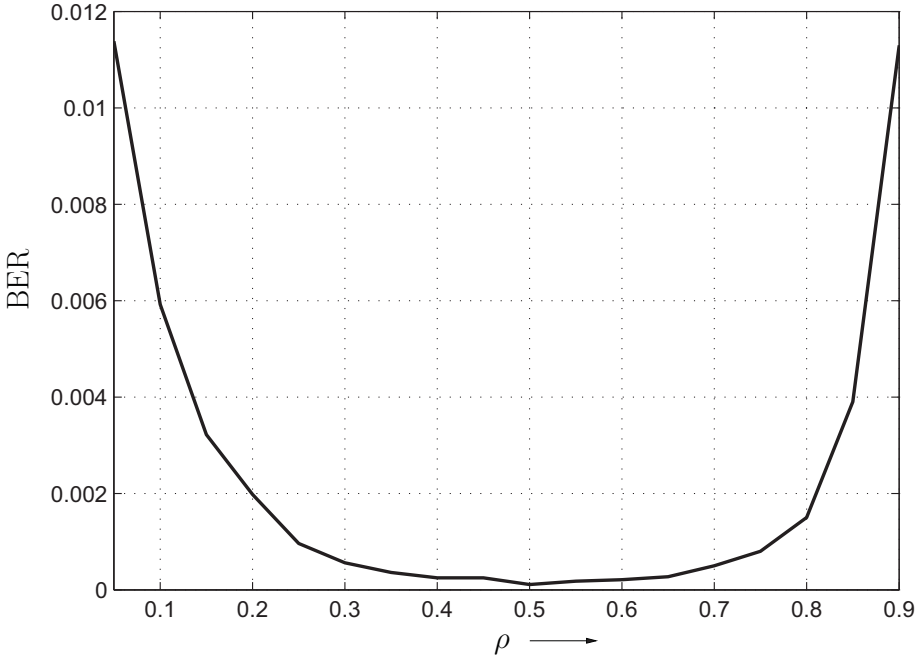

Figure 6.7: BER vs. ρ.

double differential encoding at the transmitter for a fixed E_g/N_0 ($E_g/N_0 =$ 9.7 dB). The power allocation factors are optimized based on (3.24). As can be seen, the optimum position for the A&F relay is the mid-point between the source and the destination (similar to the conventional single differential case [27]). Another result which is shown in Fig. 6.7, is that the performance of dual-hop system is robust to the position of the relay around the optimal point if the optimal power allocation factors are used.

Next, we turn to the case of multi-hop relaying. Fig. 6.8 shows the effective SNR at the destination node versus $\frac{E_g}{N_0}$ for three-hop ($m = 3$) and four-hop ($m = 4$) transmission. In particular, the simulated effective SNR

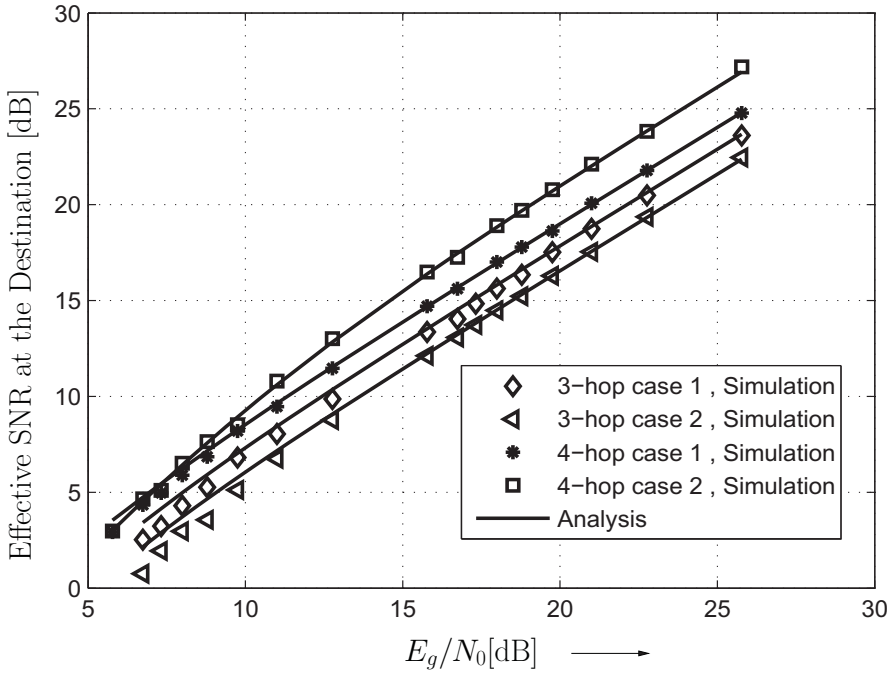

Figure 6.8: Effective SNR at the destination node for the three-hop and the four-hop case.

values at the destination node (markers) and the corresponding analytical values are compared for two different arrangements of relays. The arrangement of the relays in case 1 for $m = 3$ and $m = 4$ are $0.5 - 0.4 - 0.1$ and $0.25 - 0.25 - 0.25 - 0.25$ (normalized with respect to the length of S-D link), respectively. These arrangements in case 2 are $0.6 - 0.3 - 0.1$ and $0.1 - 0.3 - 0.2 - 0.4$ for three-hop and four-hop relaying, respectively. As Fig. 6.8 shows, the SNR calculated based on (4.9) and the simulated effective SNR are in excellent agreement for both three-hop and four-hop transmission.

Table 6.1 and Table 6.2 show the (near-) optimum transmit power allocation factors α_i obtained by means of the algorithm proposed in Section 4.2 for three-hop ($m=3$) and four-hop ($m=4$) relaying, respectively, for different relay positions. E_g/N_0 is 12.8 dB for both tables, and we chose $p = 3$ and $p = 4$ for the three-hop case and the four-hop case, respectively. The resulting values are compared with those obtained from an exhaustive search. As can be observed, the results obtained with (4.14) are close to optimal.

Table 6.1: Transmit power allocation factors α_i^* for the three-hop case ($m=3$); the first column indicates the relative positions of the relays (normalized w.r.t. the source-destination link length).

Relative position of relays	Type of optimization	α_1^*	$\alpha_2^*\varepsilon_{rx1}$	SNR
$0.1-0.1-0.8$	Proposed formula	0.11	0.06	14.95
	Exhaustive search	0.1	0.05	14.99
	Equal power	0.33	0.33	10.36
$0.1-0.2-0.7$	Proposed formula	0.12	0.18	15.52
	Exhaustive search	0.11	0.15	15.59
	Equal power	0.33	0.33	12.53
$0.1-0.6-0.3$	Proposed formula	0.09	0.75	13.73
	Exhaustive search	0.08	0.8	13.69
	Equal power	0.33	0.33	10.54
$0.33-0.33-0.33$	Proposed formula	0.52	0.30	14.20
	Exhaustive search	0.5	0.31	14.24
	Equal power	0.33	0.33	13.63
$0.4-0.4-0.2$	Proposed formula	0.59	0.34	12.90
	Exhaustive search	0.57	0.37	12.93
	Equal power	0.33	0.33	11.40

Table 6.2: Near-optimum transmit power allocation factors α_i^* for the four-hop case ($m = 4$); the first column indicates the relative positions of the relays (normalized w.r.t. the source-destination link length).

Relative position of relays	Type of optimization	α_1^*	$\alpha_2^*\varepsilon_{rx1}$	$\alpha_3^*\varepsilon_{rx2}$	SNR
$0.25 - 0.25 - 0.25 - 0.25$	Proposed formula	0.52	0.27	0.14	15.38
	Exhaustive search	0.52	0.26	0.12	15.40
	Equal power	0.25	0.25	0.25	13.95
$0.1 - 0.3 - 0.2 - 0.4$	Proposed formula	0.11	0.52	0.11	17.48
	Exhaustive search	0.10	0.52	0.11	17.48
	Equal power	0.25	0.25	0.25	16.00

Chapter 7

Conclusions and Future Work

7.1 Conclusions

In this thesis, we proposed a double-differential encoding scheme for two-hop A&F relaying in IR-UWB systems. In conventional A&F relaying systems, the length of the effective overall CIR increases in each hop. As a result, the amount of ISI impairing the received signal increases in each hop leading to a poor performance. By using double-differential encoding at the transmitter, the amount of ISI can be limited to the same level as for direct transmission, without any need to increase guard intervals between transmitted pulses. This means that with the proposed scheme, the overall system benefits from path-loss gains without any loss in data rate. After a thorough performance analysis of the proposed scheme, a closed-form solution for the optimum power allocation to the source node and the relay was derived. Simulation results showed that the proposed A&F-relaying scheme offers an excellent performance and can even compete with coherent A&F and D&F-relaying schemes that are based on S-Rake combining. Subsequently, we extended

the presented framework to the case of multi-hop relaying IR-UWB systems. A multiple-differential encoding at the source node and a single-differential decoding at each relay and at the destination node was proposed for the multi-hop case. Similar to the dual-hop case, by this means, the ISI is limited in each hop without requiring an extended guard interval. Finally, a recursive formula for the SNR at the destination node and a sub-optimal approach for finding the power allocation factors was presented for the multi-hop case. Simulation results showed the excellent performance of the near-optimum power allocation factors in the more challenging case of multi-hop relaying as well as in the dual-hop case.

7.2 Future Work

There are several possible extensions of the work presented in this thesis and these are listed below.

- In this thesis, we have assumed that only one relay participates in each hop. Considering more than one relay e.g., two relays in each hop is a topic for future work.

- A second area for further development is assuming multiple antennas at the transmitter and receivers of all nodes and employing space-time codes to improve the reliability of data transmission.

- The effective noise at the destination is in general non-Gaussian and thus, finding a closed-form expression for BER seems difficult. Therefore, we have focused on the effective SNR at the destination node as

performance measure in this thesis. Finding the distribution of the noise at the destination is an interesting area for future research.

Bibliography

[1] D. Porcino and W. Hirt. Ultra-wideband radio technology: Potential and challenges ahead. *IEEE Commun. Mag.*, 41(7):66–74, July 2003.

[2] S. Roy, J. R. Foerster, V. S. Somayazulu, and D. G. Leeper. Ultrawideband radio design: The promise of high-speed, short-range wireless connectivity. *Proc. IEEE*, 2(92):295–311, Feb. 2004.

[3] Liuqing Yang and G.B. Giannakis. Ultra-wideband communications: An idea whose time has come. *IEEE Signal Processing Mag.*, 21(6):26–54, Nov. 2004.

[4] R. A. Scholtz, D. M. Pozar, and W. Namgoong. Ultra-wideband radio. *EURASIP J. Applied Signal Processing*, 2005(3):252–272, 2005.

[5] Federal Communications Commission (FCC). Revision of part 15 of the commission's rules regarding ultra-wideband transmission systems. First Report and Order, ET Docket 98–153, FCC 02–48; Adopted: February 2002; Released: March 2003.

[6] Maria-Gabriella Di Benedetto, Thomas Kaiser, Andreas F. Molisch, Ian Oppermann, Christian Politano, and Domenico Porcino. *UWB Com-*

munication Systems – A Comprehensive Overview. Hindawi Publishing Corporation, 2006.

[7] ECMA. Standard ECMA-368: High rate ultra wideband PHY and MAC standard. First Edition, Dec. 2005.

[8] R. Fisher, R. Kohno, M. McLaughlin, and M. Welbourn. DS-UWB physical layer submission to IEEE 802.15 Task Group 3a. Document Number P802.15-04/0137r4, IEEE P802.15, Jan. 2005.

[9] IEEE P802.15–TG4a. Part 15.4: Wireless medium access control (MAC) and physical layer (PHY) specifications for low-rate wireless personal area networks (LR-WPANs): Amendment to add alternate PHY. Jan. 2007.

[10] M. Win and R. Scholtz. Impulse radio: how it works. *IEEE Commun. Lett.*, 2(1):36–38, Jan. 1998.

[11] Time Domain Corporation. Comments of time domain corporation, docket 98-154. in the matter of revision of part 15 of the FCC's rules regarding ultra-wideband transmission systems. 1998.

[12] M.Z. Win and R.A. Scholtz. On the energy capture of ultrawide bandwidth signals in dense multipath environments. *IEEE Commun. Lett.*, 2(9):245–247, Sep 1998.

[13] A. Rajeswaran, V.S. Somayazulu, and J.R. Foerster. Rake performance for a pulse based UWB system in a realistic UWB indoor channel. In

Proc. IEEE Int. Conf. Commun. (ICC), volume 4, pages 2879–2883, May 2003.

[14] Ning He and C. Tepedelenlioglu. Performance analysis of non-coherent UWB receivers at different synchronization levels. *IEEE Trans. Wireless Commun.*, 5(6):1266–1273, June 2006.

[15] A.A. D'Amico and L. Taponecco. A differential receiver for UWB systems. *IEEE Trans. Wireless Commun.*, 5(7):1601–1605, July 2006.

[16] D. Cassioli, M.Z. Win, F. Vatalaro, and A.F. Molisch. Performance of low-complexity RAKE reception in a realistic UWB channel. In *Proc. IEEE Int. Conf. Commun. (ICC)*, volume 2, pages 763–767, May 2002.

[17] Shiwei Zhao, Huaping Liu, and Zhi Tian. A decision-feedback autocorrelation receiver for pulsed ultra-wideband systems. In *Proc. IEEE Radio and Wireless Conf.*, pages 251–254, Sept. 2004.

[18] J. Romme and G. Durisi. Transmit reference impulse radio systems using weighted correlation. In *Proc. Int. Workshop on Ultra Wideband Systems*, pages 141–145, May 2004.

[19] Nan Guo and R.C. Qiu. Improved autocorrelation demodulation receivers based on multiple-symbol detection for UWB communications. *IEEE Trans. on Wireless Commun.*, 5(8):2026–2031, Aug. 2006.

[20] W.P. Siriwongpairat, Weifeng Su, Zhu Han, and K.J.R. Liu. Employing cooperative diversity for performance enhancement in UWB communi-

cation systems. In *Proc. IEEE Wireless Commun. Networking Conf. (WCNC)*, volume 4, pages 1854–1859, April 2006.

[21] J. Kan, J. Mietzner, C. Snow, and R. Schober. Enhancement of the ECMA-368 UWB system by means of compatible relaying techniques. In *Proc. IEEE Int. Conf. on Ultra-Wideband (ICUWB)*, volume 2, pages 63–67, Sept. 2008.

[22] A. Sendonaris, E. Erkip, and B. Aazhang. User cooperation diversity-Part I. System description. *IEEE Trans. on Commun.*, 51(11):1927–1938, Nov. 2003.

[23] A. Sendonaris, E. Erkip, and B. Aazhang. User cooperation diversity-Part II. Implementation aspects and performance analysis. *IEEE Trans. on Commun.*, 51(11):1939–1948, Nov. 2003.

[24] J. Nicholas Laneman. *Cooperative Diversity in Wireless Networks: Algorithms and Architectures*. PhD thesis, Massachusetts Institute of Technology, September 2002.

[25] J.N. Laneman, D. N. C. Tse, and G.W. Wornell. Cooperative diversity in wireless networks: Efficient protocols and outage behavior. *IEEE Trans. on Inf. Theory*, 50(12):3062–3080, Dec. 2004.

[26] J.N. Laneman and G.W. Wornell. Energy-efficient antenna sharing and relaying for wireless networks. In *IEEE Wireless Communications and Networking Conference, (WCNC)*, volume 1, pages 7–12 vol.1, 2000.

[27] Q. Zhao and H. Li. Differential modulation for cooperative wireless systems. *IEEE Trans. on Signal Processing*, 55(7):2276–2283, May 2007.

[28] A. Sendonaris, E. Erkip, and B. Aazhang. End-to-end performance of transmission systems with relays over Rayleigh-fading channels. *IEEE Trans. on Commun.*, 6(2):1126–1131, Nov. 2003.

[29] M.O. Hasna and M.-S. Alouini. Harmonic mean and end-to-end performance of transmission systems with relays. *IEEE Trans. on Commun.*, 52(1):130–135, Jan. 2004.

[30] C. Abou-Rjeily and N. Daniele J.-C. Belfiore. On the amplify-and-forward cooperative diversity with time-hopping ultra-wideband communications. *IEEE Trans. Commun.*, 56(4):630–641, April 2008.

[31] S. Zhu, K. Leung, and A. Constantinides. Distributed cooperative data relaying for diversity in impulse-based UWB ad-hoc networks. *IEEE Trans. Wireless Commun.*, 8(8):4037–4047, August 2009.

[32] K. Maichalernnukul, T. Kaiser, and F. Zheng. On the performance of coherent and noncoherent UWB detection systems using a relay with multiple antennas. *IEEE Trans. Wireless Commun.*, 8(7):3407–3414, July 2009.

[33] M.K. Simon and D. Divsalar. On the implementation and performance of single and double differential detection schemes. *IEEE Trans. Commun.*, 40(2):278–291, Feb 1992.

[34] A.F. Molisch, J.R. Foerster, and M. Pendergrass. Channel models

for ultrawideband personal area networks. *IEEE Wireless Commun.*, 10(6):14–21, Dec. 2003.

[35] S. Ghassemzadeh and V. Tarokh. A statistical model for in-home UWB channels. In *Proc. IEEE Int. Conf. on Ultra Wideband Systems and Technology (ICUWB)*, pages 59–64, 2002.

[36] J Kunisch and J Pamp. Measurements results and modeling aspects for the UWB radio channels. In *Proc. IEEE Int. Conf. on Ultra Wideband Systems and Technology (ICUWB)*, pages 19–23, 2002.

[37] John Proakis. *Digital Communications*. New York: McGraw Hill, 4 edition, 2001.

[38] Marvin K. Simon and Mohamed-Slim Alouini. *Digital Communication Over Fading Channels*. Hoboken, New Jersey: John Wiley & Sons, Inc., 2 edition, 2005.

[39] S. Gezici, H. Kobayashi, H. V. Poor, and A. F. Molisch. Performance evaluation of impulse radio UWB systems with pulse-based polarity randomization. *IEEE Transactions on Signal Processing*, 53:2537–2549, 2005.

Appendix A

Calculation of the Variance of the Noise at Each Relay for Multi-hop Transmission

A.1 Calculation of $\sigma^2_{z'_{i+1}}$

From (2.6), (2.8), and (4.4) we can divide z'_{i+1} into its components as follows

$$z'_{i+1}[k] = z'_{i+1,1}[k] + z'_{i+1,2}[k] + z'_{i+1,3}[k], \tag{A.1}$$

where $z'_{i+1,1}[k]$, $z'_{i+1,2}[k]$, and $z'_{i+1,1}[k]$ are defined by

$$\begin{aligned} z'_{i+1,1}[k] &= \hat{x}_{i+1}[k]\sqrt{A_{i+1}\alpha_{i+1}E_g} \\ &\quad \times \sum_{j=0}^{N_f-1} \int_{kT_s}^{kT_s+T_i} n_{i+1}(t - T_s) w_{rx,i+1}(t - jT_f - kT_s)dt, \end{aligned} \tag{A.2}$$

$$z'_{i+1,2}[k] = \hat{x}_{i+1}[k-1]\sqrt{A_{i+1}\alpha_{i+1}E_g} \times \sum_{j=0}^{N_f-1}\int_{kT_s}^{kT_s+T_i} n_{i+1}(t)w_{rx,i+1}(t-jT_f-(k-1)T_s)dt, \quad (A.3)$$

$$z'_{i+1,3}[k] = \int_{kT_s}^{kT_s+T_i} n_{i+1}(t)n_{i+1}(t-T_s)dt. \quad (A.4)$$

Replacing $\hat{x}_{i+1}$ from (4.1) in (A.3), through the same lines, the variance of $z'_{i+1}[k]$ can be calculated. The variance of the noise terms $z'_{i+1,1}[k]$, $z'_{i+1,2}[k]$, and $z'_{i+1,3}[k]$ can be approximated as

$$\begin{aligned}\sigma^2_{z'_{i+1,1}} &\approx E\{\hat{x}^2_{i+1}[k]\}\beta_{i+1}\frac{N_0}{2} = (\tilde{\beta_i}^2+\sigma_i^2)\beta_{i+1}\frac{N_0}{2},\\ &\sigma^2_{z'_{i+1,2}} = \sigma^2_{z'_{i+1,1}}, \quad \sigma^2_{z'_{i+1,3}} = \sigma^2_{z'_{1,3}} = \frac{WT_iN_0^2}{2}. \end{aligned} \quad (A.5)$$

Thus, the variance of z'_{i+1}, $\sigma^2_{z'_{i+1}}$, is calculated as $\sigma^2_{z'_{i+1}} \approx (\tilde{\beta}_i^2+\sigma_i^2)\beta_{i+1}N_0+\frac{WT_iN_0^2}{2}$.

A.2 Calculation of $\sigma^2_{z_{i+1}}$

Plugging $\hat{x}_\nu$ from (4.1) into (4.4), yields

$$\hat{x}_{i+1}[k] = \beta_{i+1}(\tilde{\beta_i}^2\overbrace{q_{m-i+1}[k]q_{m-i+1}[k-1]}^{q_{m-i}[k]}+\tilde{\beta}_i(q_{m-i+1}[k]z_i[k-1] +q_{m-i+1}[k-1]z_i[k]) + z_i[k]z_i[k-1]) + z'_{i+1}[k]. \quad (A.6)$$

Comparing (A.6) with (4.5), we obtain

$$\begin{aligned} z_{i+1}[k] &= \beta_{i+1}(\tilde{\beta}_i \cdot (q_{m-i+1}[k]z_i[k-1] + q_{m-i+1}[k-1]z_i[k]) \\ &\quad + z_i[k]z_i[k-1]) + z'_{i+1}[k]. \end{aligned} \tag{A.7}$$

The first two terms in (A.7) are not mutually independent, and we need to calculate their correlation in order to find the variance of $z_{i+1}[k]$.

From (A.7) we observe that

$$\begin{aligned} q_{m-i+1}[k]z_i[k] = \beta_i(\tilde{\beta}_{i-1}(&q_{m-i+2}[k-1]z_{i-1}[k-1] \\ &+ q_{m-i+2}[k]z_{i-1}[k]) + q_{m-i+1}[k]z_{i-1}[k]z_{i-1}[k-1]) \\ &+ q_{m-i+1}[k]z'_i[k], \end{aligned} \tag{A.8}$$

and

$$\begin{aligned} q_{m-i+1}[k-1]z_i[k-1] =& \beta_i(\tilde{\beta}_{i-1}(q_{m-i+2}[k-2]z_{i-1}[k-2] \\ &+ q_{m-i+2}[k-1]z_{i-1}[k-1]) \\ &+ q_{m-i+1}z_{i-1}[k-1]z_{i-1}[k-2]) \\ &+ q_{m-i+1}[k-1]z'_i[k-1]. \end{aligned} \tag{A.9}$$

Using the same approach as in Section 3.1, $\eta_i := E\{q_{m-i+1}[k]z_i[k]q_{m-i+1}[k-1]w_i[k-1]\}$ can be calculated as follows

$$\begin{aligned}\eta_i =\ & E\{q_{m-i+1}[k]z_i[k]q_{m-i+1}[k-1]w_i[k-1]\}\\ \approx\ & E\{\beta_i^2\tilde{\beta}_{i-1}^2 z_{i-1}^2[k-1]\}\\ & + 2E\{\beta_i^2\tilde{\beta}_{i-1}^2 q_{m-i+1}[k-1]z_i[k-1]q_{m-i+1}[k-2]z_i[k-2]\}\\ & + \tilde{\beta}_{i-1}^2\beta_i\frac{N_0}{2}.\end{aligned} \tag{A.10}$$

The last term is obtained from $E\{q_{m-i+1}[k]z_i'[k]q_{m-i+1}[k-1]z_i'[k-1]\}$. Similar to the Section 3.1, a careful look at (A.2) shows $q_{m-i+2}[k]z_{i,1}'[k]$ and $q_{m-i+2}[k-2]z_{i,2}'[k-1]$ are not mutually independent. Thus similar to (3.18), we obtain $E\{q_{m-i+1}[k]z_i'[k]q_{m-i+1}[k-1]z_i'[k-1]\} = E\{q_{m-i+2}[k]z_{i,1}'[k]q_{m-i+2}[k-2]z_{i,2}'[k-1]\} = \tilde{\beta}_{i-1}^2\beta_i\frac{N_0}{2}$.

Finally η_i can be calculated recursively as

$$\eta_i \approx\ \beta_i^2\tilde{\beta}_{i-1}^2\sigma_{i-1}^2 + 2\beta_i^2\tilde{\beta}_{i-1}^2\eta_{i-1} + \tilde{\beta}_{i-1}^2\beta_i\frac{N_0}{2}. \tag{A.11}$$

Here, we have used the approximation that for a small to moderate number of intermediate A&F relays the correlation between the noise terms $z_{i+1}'[k]$ and $z_{i+1}[k]$, cf. (4.4) and (4.5), can be neglected. According to (A.5), (A.7), and (A.11), the variance of the noise at the ith relay can also be obtained recursively as

$$\sigma_{i+1}^2 \approx \beta_{i+1}^2\left(2\tilde{\beta}_i^2(\sigma_i^2+\eta_i)+\sigma_i^4\right) + \beta_{i+1}N_0(\tilde{\beta}_i^2+\sigma_i^2) + \frac{WT_iN_0^2}{2}. \tag{A.12}$$